Biomorphic Ceramics from Wood Derived Precursors

J. Ramírez-Rico[a*], J. Martínez-Fernandez[a], M. Singh[b]

[a] *Dpto. Física de la Materia Condensada. Instituto de Ciencia de Materiales de Sevilla (ICMS). Universidad de Sevilla. Consejo Superior de Investigaciones Científicas (CSIC). Avda. Reina Mercedes S/N, 41012 Sevilla, Spain*

[2] *Ohio Aerospace Institute, 22800 Cedar Point Road, Cleveland, OH 44142, USA*

Joaquín Ramírez Rico obtained his PhD from the University of Seville in 2008, where he is currently Assistant Professor in the Solid State Physics Department at the University of Seville. He has authored more than 55 papers in peer-reviewed journals and his current interests are in natural and bioinspired material, novel structural ceramics and ceramic-matrix composites, and in-situ materials characterization using x-ray techniques.

Julián Martinez Fernandez is Professor of Solid State Physics and Materials Science, at the University of Seville, Spain, where he also serves as the Director of Research Facilities. He has published over 160 papers in peer-reviewed journals and has been the PI of over 20 nationally and internationally funded research grants. His research interests include the study of biomorphic silicon carbide, single crystal and polycrystalline zirconia and alumina, alumina-based composites, silicon nitride, electronic ceramics, ceramic joining, and single crystals fibers.

Mrityunjay Singh is Chief Scientist, Ohio Aerospace Institute, NASA Glenn Research Center, Cleveland, Ohio. He has edited/co-edited thirty eight books and five journal volumes, authored/co-authored ten book chapters/invited reviews and more than two hundred fifty papers in journals and edited volumes. He is involved with various activities in processing, manufacturing, joining and attachment technologies, and characterization of advanced ceramics and composites, lightweight cellular ceramics, environment conscious ceramics, and porous ceramic foams, high conductivity composites and graphite foams for thermal management systems, ceramic matrix composites for turbomachinery and propulsion systems, and a wide variety of materials for ultra high temperature and extreme environment applications.

* Corresponding author – Email: jrr@us.es, Tel: +34 954 550 936

Biomorphic Ceramics from Wood Derived Precursors

Materials development is driven by microstructural complexity, in many cases inspired by biological systems like bones, shells, and wood. In one approach, one selects the main microstructural features responsible for improved properties a designs processes to obtain materials with such microstructures (continuous-fiber-reinforced ceramics, porous ceramics, fibrous ceramic monoliths, etc.). In a different approach, it is possible to use natural materials directly as microstructural templates. Biomorphic ceramics are produced from natural and renewable resources (wood or wood-derived products). A wide variety of SiC based ceramics can be fabricated by infiltration of silicon or silicon alloys into cellulose-derived carbonaceous templates, providing a low-cost route to advanced ceramic materials with near-net shape potential and amenable to rapid prototyping. These materials have tailorable microstructure and properties, and behave like ceramic materials manufactured by advanced ceramic processing approaches. This review aims to be a comprehensive description of the development of bioSiC ceramics: from wood templates and their microstructure to potential applications of bioSiC materials.

Keywords: biomorphic; ceramics; wood; silicon carbide; mechanical properties; high temperature; porous materials

1 Introduction

Silicon carbide-based ceramics are interesting materials for key engineering applications, especially those requiring good thermomechanical performance and specific properties. However, in many cases SiC materials do not find extensive usage due to their high cost, as they are obtained at very high sintering temperatures and require expensive manufacturing (extrusion, molding, and machining, etc) techniques to produce complex-shaped components. For this reason, SiC ceramics are often limited to niche applications. Macroporous ceramics [1] and specifically macroporous silicon carbide materials [2] are also interesting candidates for a wide range of applications, especially in high temperature environments involving corrosive gases and high mechanical loading. Envisioned applications could be catalyst supports, thermal insulation and management, or filtration of molten metals, liquids or gases (such as in diesel particulate filters or in gasification processes). Thus, there is technological potential in any process that allows one to obtain SiC monoliths with reduced processing and machining costs, but also that enables the production of porous SiC ceramics, ideally with the same low cost attributes as outlined above.

A way to overcome these problems is to synthesize SiC ceramics by melt infiltration of a porous carbonaceous preform, typically obtained from the pyrolysis of a cast polymer, to produce Reaction Formed SiC (RFSC) [3-10], a process developed in the early 90s that is near-net shape and allows to obtain monolithic SiC materials with small amounts of unreacted carbon and silicon. The microstructure of these materials depend on the characteristics of the carbon template and are, in a way, inherited from it, so by tailoring the template and increasing its microstructural complexity, a wide variety of SiC materials could be obtained.

Biomorphic silicon carbide (bioSiC) are bio-templated SiC materials that start with a porous carbon scaffold derived from natural precursors such as wood, which is later converted into a SiC ceramic by a variety of methods, most commonly by melt infiltration. In this case, bioSiC is simply a type of reaction formed silicon carbide in which the carbon template is obtained by pyrolysis of wood, with the advantage of a complex, hierarchical microstructure that is the result of millions of years of evolution and is optimized for properties such as fluid transport or high strength to density ratios [11].

Several routes have been developed to obtain SiC ceramics starting from wood-derived carbon preforms, in a way that retains most of the microstructural features of the template. Figure 1 summarizes the three most common ones: melt-infiltration of liquid Si, vapor infiltration of Si either directly or through decomposition of SiO, or infiltration of SiO_2 sols or gel precursors that react with carbon *via* carbothermal reduction to form SiC. All three processes start with a carbon template obtained from a wood precursor that is chosen according to the desired properties of the final material, although in some works wood is impregnated with a SiO_2 precursor so carbonization and carbothermal reduction is carried out in a single step. All three routes also have in common that they are near-net-shape processes because after conversion the size and shape of the final material is equal to that of the preform, and any volume change associated with the reaction is buffered by the precursor's porosity. This makes the conversion of carbonaceous precursors into SiC a highly cost effective method to produce SiC ceramics, porous or otherwise, as any desired machining can be done to the carbon preform and only finishing will need to be performed in the final component, greatly decreasing processing costs when compared to typical sintering and hot-pressing processes that might require extensive machining with expensive diamond tools. As an example of the complexity of shapes that can be produced, Figure 2 shows some components manufactured by melt infiltration of MDF derived bioSiC/Si, where all machining was performed in the carbon stage.

From a historical point of view, the first mentions in the literature of using wood as a template for advanced materials processing is from Ota *et al*. [12] who synthesized "SiC wood" by tetraethyl-orthosilicate infiltration and later carbothermal reduction of wood chars. Byrne and Nagle made important contributions to the field by laying the groundworks of wood pyrolysis with materials applications in view, such as optimization of heating rates, densities and shrinkage ratios, as well as their effect on mechanical properties [13-15]. Later reports on biomorphic SiC are from Greil and coworkers [16-19], as well as Singh, who coined the term "Ecoceramics" to refer to this new class of wood-derived materials [20, 21]. Several general papers exist that deal with the basics of biomorphic SiC materials [19, 20, 22-24].

2 Carbon Templates from Natural Wood Precursors

2.1 Wood Structure and Composition

Wood can be considered a natural material with a complex microstructure optimized by evolution for a good strength-to-density ratio and fluid transport [25]. It is a porous material with densities in the range 0.3-0.8 g cm^{-3} depending on species. The wide variety of commercially available wood from different species, and the possibility of using industrial wood products (paper, cardboard, cellulose paste, particle and fiberboards) allows the processing of bioSiC materials with a wide range of properties depending on the targeted application.

The structure of wood has been studied in detail [26-29] and is composed of a stacking of elongated, tubular cells aligned in the tree's growth direction. Wood can be broadly classified into two groups attending on its microstructure: in softwood from gymnosperm trees such as conifers, wood is composed of only one type of cell, called tracheids, while in angiosperm wood these are surrounded by smaller sclerenchymatic cells with a distribution that is characteristic of each species. Among them, small sized, thick walled cells are responsible for the mechanical strength of wood and receive the name of libriform "fibers". In angiosperms, tracheids can have diameters over one hundred microns and are responsible for fluid transport (sap channels). Due to this structure, pore distribution in angiosperm wood is bimodal, while in wood from gymnosperm species the pore size distribution is monomodal with channels in the range of 30-50 μm. Figure 3 shows a schematic of wood from both angiosperm and gymnosperm precursors.

The structure and composition of cell walls determines the properties of wood and wood-derived products [30] and is similar for soft and hardwoods. This can be described as a lamellar or layered microstructure where each layer is composed of cellulose, hemicellulose and lignin (lignocellulose). Celluloses are long polymeric chains (up to 1 μm in length) aggregated into microfilaments normally aligned with the cell's longest dimension. Hemicelluloses are shorter chains interconnecting cellulosic microfilaments while lignin occupies the spaces left by the cellulose and hemicellulose networks.

By its very nature, wood has a highly anisotropic structure and its properties are described along three planes and their respective perpendicular directions: axial, radial and tangential (Figure 3). In addition to the presence of pores and cells, wood shows two types of macrostructures: rays and growth rings. Rays are horizontally aligned cells used for nutrient storage and radiate from the axis of the three, while growth rings are concentric rings that result from changing pore sizes due to seasonal variations in tree growth. Due to the absence of sap channels, softwoods from gymnosperms are usually referred to as non-porous, while hardwoods from angiosperms are classified according to their growth ring morphology into ring porous or diffuse porous: in ring porous hardwoods sap channels are segregated into bands while in diffuse-porous wood there is no such segregation (Figure 4) [28, 29].

2.2 Pyrolysis of Wood

Pyrolysis of wood for the production of carbon templates to be further converted into SiC ceramics is performed in inert atmospheres (typically Ar or N_2) by slowly heating the wood precursors up to temperatures in excess of 800°C. During pyrolysis the different polymeric components of wood decompose in a step-wise manner with hemicellulose breaking-down first at 200-260 °C, followed by cellulose at 240-350ºC and lignin at 280-500°C and up. Figure 5 shows typical thermogravimetric and loss rate per unit temperature curves for thermal decomposition of *Quercus rubra* (red oak) wood, exhibiting the step-wise process described earlier [14]. Labeled regions correspond to (1) loss of adsorbed water, (2) polymer decomposition of hemicellulose and (3) cellulose as well as lignin, (4) total decomposition of cellulose and decomposition of remaining lignin above 400 ºC (5). These stages more or less correspond to those described by Tang and Bacon and others [31], involving (a) the desorption of adsorbed water up to 150 ºC; (b) the splitting off of cellulose structure water between 150 and 240 °C; (c) depolymerization and breaking of C-O and C-C bonds within ring units evolving water, CO and CO_2; (d) aromatization forming graphitic layers above 400 °C. In lignocellulosic materials such as

wood the carbon-to-volatiles mass ratio increases with pyrolysis temperature, yielding ~90% carbon at 600 °C, while the rest is mostly nitrogen and oxygen, with small amount of other elements. Ash content varies with species and is between 0.5 to 3 wt. % of the carbon monoliths. Ashes from wood derived carbon contain mostly sodium, magnesium, phosphor, potassium, calcium, manganese and iron.

Since crack-free monoliths are required for use as templates in SiC ceramic synthesis, pyrolysis must be carefully controlled and performed at very low heating rates, in the range of 1ºC/min up to 400-500 °C, where most of the thermal decomposition of polymers takes place. Such a slow rate allows for gaseous reaction products to evacuate the material through the pores without building up pressure that could lead to cracking. After that slow initial stage, pyrolysis can be accelerated to rates of the order of 10-20 °C/min without affecting the integrity of the final template. This slow process has the advantage of producing high carbon yields, in the 25-30 wt. % range when compared to the initial wood mass.

It has been shown that the density of the carbon scaffold obtained by pyrolysis is proportional to that of the wood precursor, as was first observed by Byrne and Nagle as well as others [14]. Some examples of this are shown in Figure 6, where a linear fit of the form $\rho_c = \alpha\rho_{wood}$ is included. Values of the parameter α vary with pyrolysis conditions, being mostly affected by the heating rate, but is roughly ~0.8 for slow pyrolysis conditions such as those typically used to obtain preforms for Si infiltration.

Pyrolysis is accompanied by a shrinkage of the wood-carbon monolith, the extent of which is determined by the wood employed. It has been shown that shrinkage in the radial and tangential directions vary greatly from species to species, in the range of 25-40 % length reduction, while axial shrinkage is similar for all types of wood and results in ca. 20 % reduction, although these values themselves depend on the pyrolysis temperature, remaining constant over 1000 ºC (Table 1).

3 Biomorphic ceramics by melt infiltration of carbon preforms

Processing of bioSiC by melt infiltration is well documented in the literature, and protected by patents [18, 22, 24, 32-40]. Basically, it involves the infiltration of liquid silicon into the carbon preform, by heating silicon powder in contact with it at temperatures in excess of the melting point of silicon (typically > 1450°C) in vacuum. Silicon quantities well above the stoichiometric ratio to carbon are typically used to

ensure almost-complete conversion of the carbon template to SiC. During reaction, the carbon walls in the template are converted into β-SiC and the smaller pores in the template, up to a pore diameter of approximately 50 μm, are filled with residual silicon. The Si, SiC and residual carbon content of the final bioSiC/Si composite, as well as the remaining pores' size and distribution, if any, depend on the processing conditions, amount of excess Si, and the anatomy of the wooden preform.

Infiltration of SiC is a near-net shape process, as the volume expansion associated with the conversion of C into SiC is absorbed by the porous structure leaving the outer dimensions unchanged. Varela-Feria [41] performed a series of infiltrations using carbon templates shaped as parallelepipeds with sides of different lengths and measured the dimensions of the resulting bioSiC/Si materials (Figure 8), with the result that external sample dimensions did not change upon melt infiltration regardless of initial dimensions and aspect ratio.

In melt infiltration, conversion of carbon into SiC takes place by two mechanisms which are active depending on the carbon wall thickness and topology. As will be elaborated further below, the main mechanism is dissolution of carbon into the melt followed by reprecipitation of micron-sized (ca. 10 μm) β-SiC grains at the carbon-silicon interface: silicon penetrates through the carbon preform by capillary effects and reacts with the solid C spontaneously and exothermically, with an enthalpy of ΔH^0=-117.77 kJ/mol [42]. In denser areas of the carbon template the carbon density can exceed the critical limit of about 0.97 g cm^{-3} which can result in clogging of the pores preventing further SiC formation by precipitation [5-7]. In these cases solid state diffusion and reaction control the formation of SiC now at the SiC-carbon interface, resulting in the formation of a nano-grained SiC phase (< 100 nm) [24, 39, 40, 43, 44].

This mechanism is corroborated first by microstructural observations. Figure 9 shows the main microstructural features in bioSiC. Three different phases can be distinguished: polycrystalline SiC shows intermediate contrast under backscattered electrons in the SEM (A, B and C), while Si appears light grey and residual carbon appears black. Micron-sized SiC grains can be found inside channels where Si is majority (large channels with diameter over 5 μm). In small channels where Si is usually depleted in the reaction, a layer of nano-sized SiC grains can be observed at the interface between unreacted carbon and micron-sized SiC grains, which are typically majority (panel D). Nanosized SiC is found at SiC-carbon interfaces, but not at SiC-Si interfaces. Where thin carbon walls surrounding the

large channels existed, large grained SiC appears forming layers. Occasionally these layers are discontinuous and even some isolated SiC grains are observed (figure 9B, marked with arrows). At the SiC-carbon interfaces nanosized grains can be found forming rosettes which is typical of diffusion-controlled growth [45], while micron-sized SiC grains are faceted, typical of a precipitation mechanism. Figure 10 shows transmission electron microscopy images of the interfaces in the region of narrow and large channels, along with selected area diffraction patterns, corroborating the previous observations.

Microstructural parameters of the resulting materials are inherited from the wood template and therefore show great variability, which means that they can be tailored by adequate selection of the precursor. Table 1 shows several parameters such as density, silicon volume fraction or porosity for melt infiltrated bioSiC from different precursors and in comparison with the carbon template.

The β-SiC formation has been shown to follow first order kinetics, so the concentration of each phase can be modelled using:

$$[C_i] = \left[C_i^f\right] + \left(\left[C_i^0\right] - \left[C_i^f\right]\right) \exp kt$$

Where k is the reaction constant and C_i is the concentration of phase i. $\left[C_i^f\right]$ final concentration for each phase, which is not necessarily zero since there is excess Si as well as unreacted carbon in the final material. $\left[C_i^0\right]$ is the initial concentration of phase i. Figure 11 shows the evolution of each phase's concentration with time, along with fits using the previous equation, from a work by Varela-Feria *et al*. [39]. In their work, the reaction constant was determined as k=1.8 · 10^{-2} s^{-1}, similar to that measured by Pampuch et al., who studied the SiC formation process by reaction of bundles of C fibres 4-6 μm in diameter with liquid Si at 1422 °C and 1439 °C [46, 47], and determined the reaction constant k using DTA analysis. The possibility of a diffusion-controlled reaction rate is not compatible with the measured k values, as using data from Hon et al. [45, 48] and assuming the reaction was controlled by diffusion through the SiC layer, a value in the range of $k = 1.0 - 3.0 \cdot 10^{-10} s^{-1}$ would be expected.

4 Macroporous SiC Ceramics

4.1 Residual Si Removal

In the processing of wood-derived SiC ceramics obtained by melt infiltration Si is usually added in excess with respect to amount needed for stoichiometric reaction, which results in the presence of residual Si filling some or all of original channels of the wood precursor. Removal of this residual Si results in a macroporous SiC ceramic with elongated, anisotropic and hierarchical porosity that is interesting for a wide range of applications, some of which are discussed in section 6. Several techniques are available for removal of this secondary phase, the one most often used being chemical etching using a mixture of HNO_3 and HF in a molar ratio of 1.67 according to the following reactions:

$$3Si + 4HNO_3 \rightarrow 3SiO_2 + 4NO + 4H_2O$$
$$SiO_2 + 4HF \rightarrow SiF_4 + 2H_2O$$

The reaction has been shown to be diffusion limited and the etching rate R follows that of a boundary layer problem:

$$R \sim (Dt)^{-1/2}$$

The evolution of the reaction front as a function of etching time is shown for transverse sections in Figure 12 while Figure 13 [49, 50] shows the reaction front advance as well as the reaction rate in a log scale. The differences in etching rates for the different directions with respect to the growth axis of the wood precursor were attributed to an effective diffusion coefficient D_{eff} which depends on the apparent porosity in each direction due to the anisotropic permeability of the porous bioSiC.

The porosity of bioSiC after removal of remaining silicon resembles that of the original wood precursor, however due to the volume expansion associated with the $C + Si(l) \rightarrow SiC$ reaction, pores with sizes smaller than $\sim 1\ \mu m$ close during the reactive infiltration step and are therefore not present in the porous bioSiC scaffold. Pappacena *et al.* used mercury intrusion porosimetry to study the pore diameter distribution in both carbon scaffolds obtained from different wood precursors and resulting porous SiC materials and found a total porosity reduction of ~10%, depending on species, mostly derived from the closure of pores < 1 μm during the infiltration step [51]. The large macroporosity, with diameters 10 μm and larger, remained basically unchanged (Figure 14). Connectivity

between axial pores is also preserved after the infiltration and etching steps, as demonstrated by x-ray micro-computed tomography (Figure 15) [52].

4.2 Gas-Phase Infiltration

In an attempt to obtain porous SiC materials without residual silicon in a one step process, several authors have infiltrated carbon preforms with silicon-containing vapours at high temperatures: typical reactants such as silicon vapour [18, 53, 54], SiO [54-56] or methyltrichlorosilane (MTS, CH_3SiCl_3) [57-59], among others. Some of the possible reactions involved are:

$$C(s) + Si(g) \rightarrow SiC$$

$$2C + SiO \rightarrow SiC + CO$$

$$3C + 2SiO \rightarrow 2SiC + CO_2$$

$$C + (1+x)CH_3SiCl_3 + 2H_2 \rightarrow SiC + xSiC + 3(1+x)HCl + CH_4$$

In the previous reactions it is worth noting that the molar ratio of formed SiC to reacted carbon is different for each vapour reactant that can be used. In the case of Si-vapour infiltration the SiC:C molar ratio is 1:1, where for SiO vapour infiltration the ratio is between 1:2 and 2:3. For reaction with MTS the ratio is (1+x):1, meaning that reaction with MTS will both covert the carbon into SiC but also deposit an additional molar fraction *x* of SiC. Therefore, the microstructure of the resulting bioSiC material and in particular parameters such as cell wall thickness or total density can be tailored by adequate selection of the gas phase reactant, as was shown by Greil *et al.* [60], their results summarized in table 2. Figure 16 shows the microstructure of cellular SiC obtained from Si-vapour infiltration of pine biochar. It is worth noting that a similar route can be used to obtain other biomorphic carbides, such as titanium carbide through a mixture of $TiCl_4$/methane/hydrogen [61-63].

4.3 Carbothermal Reduction of SiO_2 and Related Precursors

A third route to biomorphic SiC cellular materials is the infiltration of SiO_2 or silica-forming gel-precursors such as TEOS into the carbon template, followed by carbothermal reduction at high temperature in an inert atmosphere, a procedure first described by Ota [12] and later expanded by other authors [64-71], with the following global reaction:

$$SiO_2 + 2C \rightarrow SiC + CO_2$$

The resulting material then retains the microstructure of the precursor, but with additional surface modifications inside the porous structure such as formation of SiC whiskers and surface roughening. Carbothermal reduction of TiO_2 and ZrO_2 sols have also been used for the fabrication of TiC and ZrC biomorphic materials, respectively [71, 72].

4.4 Porous Oxide Ceramics

The same procedure described in the previous section can be used to process porous oxide ceramics that mimic the microstructure of the carbon template, by simply substituting the carbothermal reaction step with a simple calcination in air or an oxidizing atmosphere. For instance, Ota *et al.* [73] and Mizutani *el al.* [74] infiltrated carbon templates with metal alkoxides such as titanium isopropoxide, aluminum isobutoxide and zirconium *n*-propoxide to obtain porous, biomorphic ceramics of TiO_2, Al_2O_3 or ZrO_2, respectively, in a similar process as that described by Singh and Yee [75] and in a series of papers by Cao, Rambo and others [76-79]. A perhaps striking development is the work performed by Tampieri *et al.* who produced biomorphic, porous hydroxyapatite from rattan templates for bone substitution applications [80-82]. The reader is referred to those references for a comprehensive description of the experimental procedures and resulting properties.

4.5 Porous SiC as the Ceramic Preform for Metal-Matrix Composites

Although out of the scope of this review, it is interesting to note that many researchers have used the porous SiC scaffolds described previously to obtain metal-matrix composites (MMCs) in which the ceramic phase is essentially continuous, by means of different approaches. To give the reader a brief survey, Zollfrank *et al.* [83] as well as Herzog *et al.* [84] were some of the first to produce bioSiC/Al composites by means of squeeze casting, while Wilkes *et al.* produced CMCs using an Al-Si-Mg alloy using a gas pressured liquid metal infiltration furnace [85]. Further, they measured their mechanical properties [86] as well as load partitioning among the phases using *in-situ* diffraction experiments [87] and performed detailed investigations on their microstructure by means of x-ray computed micro tomography [52]. Copper-SiC composites have also been fabricated by electroplating targeting thermal applications by Pappacena *et al.* [88, 89].

5 Mechanical Properties

5.1 Room Temperature

Room temperature properties of bioSiCp/Si and bioSiCp have been thoroughly studied by several authors, and Table 2 summarizes some of their findings. Peter Greil's group was

one of the first to report on mechanical properties, first of melt-infiltrated bioSiC/Si and in comparison to the properties of the carbon preform [16, 60] and then of porous bioSiCp obtained by gas infiltration [18, 53, 54]. They were first to realize that, especially in bending, fracture strength not only depended on macroscopic parameters (density, volume fractions, pore size, etc.) but was highly influenced by the presence of macrostructural features such as rays and growth rings in the wood precursor. Gutierrez-Mora *et al.* used indentation to measure hardness of Eucalyptus, Beech and Pine derived bioSiCp/Si [90]. Presas, Llorca, Pastor and others studied the bending strength and fracture toughness of several bioSiCp/Si materials derived from hardwood that possessed aligned porosity due to unfilled sap channels [91-93], while Park *et al.* surveyed the bending and compressive strength as a function of precursor density for bioSiCp/Si synthesized by a variety of precursors [94, 95]. Hou *et al.* measured bending strength as a function of infiltration time in an attempt to verify a possible effect on the material's final properties [96]. Kaul, Faber *et al.* measured the mechanical properties (Elastic modulus, compressive strength and fracture toughness) of porous bioSiCp from different precursors [97] and used nanoindentation to measure hardness and elastic moduli of individual phases (C, SiC) in the material [98].

5.2 High Temperature

High temperature mechanical behavior has been extensively studied in bioSiC/Si composites as one of the proposed applications is as high temperature structural materials. The high temperature behavior in compression has been summarized by Martinez-Fernandez *et al.* [99], who compared high temperature creep and compressive strength of bioSiC/Si from eucalyptus wood with several commercial siliconized SiC materials: reaction formed silicon carbide (RFSC) is a Si/SiC composite similar to bioSiC, obtained by reactive infiltration of polymer derived carbon preforms, which is isotropic and contains a very high fraction of SiC; reaction bonded SiC (RB-SiC) is a SiC/Si composite obtained from reactive infiltration of a mixture of C and SiC powders. BioSiC/Si was deemed superior in terms of strength to both commercial compositions when load was applied parallel to the axial direction, determined by the growth direction of the original wood precursor. Figure 18 shows stress vs. strain curves in compression for a variety of siliconized SiC materials at temperatures where the load carrying ability of the residual Si was deemed negligible. It is remarkable that bioSiC shows the highest compressive strength despite having the lowest SiC content as a fraction of volume, an observation that was attributed to the special microstructure derived from the original wood precursor, where the SiC forms a continuous phase as opposed to for example RBSC.

Figure 19 shows the high temperature compressive strength of bioSiC obtained from different precursors in the temperature range of 1000-1450 °C, as a function of the volume fraction of SiC. In a first approximation, compressive strength can be fitted to a relationship of the type;

$$\frac{\sigma_{bioSiC}}{\sigma_{SiC}} = \left(\frac{\rho_{bioSiC}}{\rho_{SiC}}\right)^{m}$$

Where σ_{bioSiC} is the compressive strength and ρ_{bioSiC} is the density of the bioSiC material. In the same way, σ_{SiC} is the compressive strength and ρ_{SiC} the density of fully dense sintered SiC. The compressive strength increases with SiC content and is higher when the load is applied along the axial direction, although this anisotropy is less pronounced for bioSiC materials containing a large fraction of SiC. As a comparison the strength of commonly employed siliconized SiC materials is included [5, 100, 101].

The effect of the microstructure on strength was rationalized in terms of a Minimum Solid Area (MSA) model [102, 103] which was deemed more suitable than cellular models often applied to describe the mechanical behavior of wood [104]. Figure 20 shows the prediction of the MSA model for pore distributions of different shapes and stacking patterns, along with experimental results for different types of BioSiC and siliconized SiC materials. It was clear that, when compared to the strength of fully dense SiC, a cubic stacking of cylindrical pores compressed parallel or perpendicular to the cylinders' axis described the behavior of bioSiCp compressed in the axial and radial directions, respectively. RFSC behaved closer to a stacking of spherical pores while RBSC had a behavior in the range predicted for a stacking of spherical particles, in accordance to their microstructural features.

Limited studies of creep in bioSiC have been performed [36, 99], which found that temperatures in excess of 1600ºC were required to observe any type of steady-state creep (Figure 21), contrary to the case of siliconized SiC materials such as RBSC or RFSC which crept at strain rates in the range of 10^{-7}-10^{-8} s^{-1} for compressive stresses of 100-300 MPa at 1300°C. BioSiC made from eucalyptus crept at rates below their estimated detection limit of 10^{-9} s^{-1}.

5.3 Erosion and Wear

Only limited investigations in the erosion and wear properties have been reported. De Arellano-López *et al.* [105] studied erosion and strength degradation of biomorphic SiC from eucalyptus and pine by solid erosion tests using 63-390 μm SiC particles at 100 m/s as erodent, impacting at an angle of 90ºC into a surface perpendicular to the axial direction in bioSiCp, observing erosion rates in the range of 10 mg per gram of impacting erodent, an order of magnitude higher than siliconized SiC materials with a much larger SiC volume fraction, suggesting that cleavage in the Si phase and intergranular cracking in the SiC phase of bioSiC made it more susceptible to erosion than RBSiC or hot-pressed SiC which showed a larger proportion of intragranular erosion. Nevertheless, strength degradation after erosion was measured in bending and while for reaction bonded or hot-pressed SiC the reduction in strength was in the range 30-50%, it was limited to 25% in Eucalyptus-derived SiC.

Vera *et al.* measured wear rates using ball-on-disk experiments with Si_3N_4 as a counterface and found an almost two orders of magnitude difference in wear rates, depending on SiC content, when compared to hot-pressed SiC. Wear rates for softwood derived SiC were as high as 10^3 mm^3/MJ, whereas a value of 10 mm^3/MJ was measured for hot-pressed SiC. Hardwood derived bioSiC with a 50-60% SiC fraction showed wear rates ca. 10^2 mm^3/MJ.

6 Applications

The unique microstructure of biomorphic SiC, derived from the wood precursor used as a starting template is interesting in areas were a hierarchical or directional porosity is desired, and therefore several applications for biomorphic SiC as a structured porous ceramic have been proposed and/or are under development [24]. For instance, it has been found that the high surface area and elongated nature of the porosity makes bioSiCp an interesting catalyst carrier, especially for high temperature reactions such as partial oxidation of methane to syngas [106], cellulose conversion to hydrogen [107] using Ni particles, or catalytic combustion of hydrogen [108] but also combined with zeolites to form structured monoliths for sorption and catalysis [109, 110].

Porous bioSiCp has also been proposed as a high temperature gas filtration material, targeting applications such as coal gasification for syngas production, as it exhibits relatively high permeability range (10^{-6}-10^{-4} m^3 N^{-1} s^{-1}) [111] depending on porosity, while maintaining good bending strength at targeted filtration temperatures of 800°C [112]. Pilot studies using candles made of MDF-derived bioSiC performed by Alonso-Farinas *et al.*

[113] determined that flow velocities for gas filtration can be increased two-to three fold when compared to commercial SiC filtering elements.

The vascular nature of wood derived bioSiC porous materials make them interesting candidates for medical implants, specifically in cortical and load-bearing bone replacement where more conventional bioactive glasses and isotropic porous materials cannot be used due to their lack of mechanical strength. Bare porous bioSiC has been shown to be as non-cytotoxic and biocompatible as Ti6Al4V or Thermanox (c), as well as to promote bone ingrowth in *in-vivo* compatibility tests when implanted in rabbits' femur condyle [114]. Nevertheless, a range of surface treatments have been tested to enhance bioSiC bioactivity, such as pulsed-laser deposited hydroxyapatite and CaP bioglass coatings [115-118], chemical functionalization and bioactivation [119] or electrodeposition of nanostructured hydroxyapatite/collagen layers [120].

In a recent study, a two-part device which incorporated porous bioSiC as the load-bearing material was studied as potential implants for long-bone prostheses and tested *in-vivo* in sheep [80]. The device consisted of a hollow cylindrical layer of sipo-derived bioSiC intended to support most of the implant mechanical load by mimicking the outer, cortical structure of bone. Surface bioactivation was carried out by means of collagen and nano-hydroxyapatite (HA) deposition, which resulted in a uniform coating. The inside of the cylinder was filled with a bio-hybrid HA/collagen composite intended to support trabecular bone growth. This study showed the safety, feasibility, and potential of this scaffold in vivo in a sheep model. In particular, the use of BioSiC+HA/collagen combined with bone marrow stem cells showed the highest value of bone-to-implant contact and new bone growth inside the scaffold.

Recently, a growing interest in new carbon materials for energy storage applications, especially as battery or supercapacitor electrodes has sparked the development of carbide-derived carbons [121-124], in which a carbide is converted into carbon in through high temperature reaction with gaseous chlorine. Among this field, biomorphic materials have found interest as precursor for hierarchically porous carbide-derived carbons, either from SiC [125-127] or TiC [63, 128].

7 Concluding Remarks

As we have shown, biomorphic ceramics are an exciting family of SiC materials that enable many applications due to their combination of low processing costs, formability, tailorable

properties and excellent thermomechanical performance in high temperature environments. By using wood as the initial template, highly complex microstructures can be obtained, and porous SiC ceramics with hierarchical porosity can be obtained. Since the process is near net-shape, biomorphic SiC can be processed into relatively complex shapes cheaply. All these advantages make them interesting candidates for a wide range of technological applications including catalyst supports, filtration elements in combustion environments, o biomedical devices, to name a few.

Acknowledgements

Joaquin Ramirez-Rico and Julian Martinez-Fernandez gratefully acknowledge support from the Ministerio de Economía, Industria y Competitividad (MINECO), under grants MAT2016-76526-R and MAT2013-41233-R. We also thank F. M. Varela-Feria and J. Quispe for fruitful discussions and for their help in preparing some of the figures.

Figure Captions

Figure 1. Different routes to biomorphic SiC materials and composites by infiltration of a porous carbon precursor.

Figure 2. Some components made of melt-infiltrated bioSiCp, in this case using MDF as a precursor. Courtesy of biomorphic EBT.

Figure 3. (top) Schematic of wood structure and definition of the three main planes used to describe for both gymnosperm and angiosperm specimens. (bottom) Actual microstructure determined from optical microscopy in sections along the three planes. From [28].

Figure 4. Axial sections of wood from three different species, a non-porous softwood (white pine), a ring porous hardwood (red oak) and a diffuse porous hardwood (tulip tree), highlighting the three different types of growth rings. Rays are signaled by red arrows, while growth rings are marked by white arrows. Adapted from [28].

Figure 5. Weight loss (TGA) analysis of the pyrolysis of *Quercus rubra* (red oak) wood along with the rate of loss with temperature. Labeled regions correspond to (1) loss of adsorbed water, (2) polymer decomposition of hemicellulose and (3) cellulose as well as lignin, (4) total decomposition of cellulose and decomposition of remaining lignin above 400 ºC (5).

Figure 6. Final carbon density as a function of wood density before pyrolysis. A linear fit to the data is included. Solid points correspond to data by Byrne and Nagle while hollow points correspond to our own unpublished data.

Figure 7. SEM micrographs of axial sections of carbon obtained through pyrolysis of different wood precursors, highlighting the resemblance of the carbon scaffold microstructure to that of the original wood precursor.

Figure 8. Final dimensions of melt-infiltrated beech-derived carbon as a function of initial dimension, for parallelepipeds of different sizes and aspect ratios. The straight line has a slope of one, indicating that the dimensions of the original templates were conserved.

Figure 9. SEM micrographs of bioSiC obtained from beech wood: A) Low magnification B) High magnification micrograph of SiC-Si interfaces. C) High magnification micrograph of

SiC-carbon interfaces. D) TEM micrograph of a SiC-carbon interface showing a rosette of nano-sized grains [39].

Figure 10. Transmission electron microscopy images and associated diffraction patterns of melt infiltrated bioSiC in the vicinity of narrow channels (left) and large channels (right), highlighting the differences stated in the text. In narrow channels a SiC/carbon interface is formed with a layer of nanosized grains, whereas in large channels SiC/silicon interfaces are formed between large (micron-sized) grains.

Figure 11. Time dependent phase fractions of carbon, silicon and SiC for silicon melt infiltration of wood-derived carbon preforms [39].

Figure 12. SEM micrographs of transverse sections of porous bioSiC for different etching times, from [49]. From left to right and top to bottom, etching times are 0.5, 1, 2, 6, 18 and 64 h.

Figure 13. Etching rate obtained from SEM micrographs of sections of porous bioSiC for different etching times, for sipo wood [49] and MDF derived bioSiCp [50]. The etching rate follows a $t^{-1/2}$ law that confirms the diffusion limited nature of the reaction.

Figure 14. Pore size distributions and porosities of (a) carbon samples pyrolyzed to 1000 ◦C and (b) silicon carbide samples derived from carbon pyrolyzed to 1000 ◦C from five wood precursors as determined by mercury porosimetry. Curves are offset by (a) 20 volume% and (b) 30 volume% for ease of viewing. From [51].

Figure 15. Transverse cross section from a 3D reconstruction obtained by x-ray micro-computed tomography of porous bioSiC. Each colored region represents an interconnected structure, from [52].

Figure 16. Microstructure of porous bioSiC obtained from Si vapor infiltrated-pine char. From [53].

Figure 17. Young's Modulus and bending strength of carbon preforms and bioSiC/Si composites obtained from Balsa, Pine, Maple, Oak, Beech and Ebony precursors, as a function of density, when the load was applied in the axial or radial orientations. From [16]

Figure 18. High temperature stress vs. strain plots for Refel RBSiC (89% SiC), Cerastar RB (80% SiC), Cerastar RX (74% SiC), LS-RFSiC (91% SiC) and bioSiC (63% SiC, fabricated from eucalyptus wood) in the axial direction. A) 1000 °C and B) 1330 °C. From [22].

Figure 19. Compressive strength of different siliconized SiC materials compared to the strength of sintered SiC as a function of SiC fraction in the material. BioSiC obtained from wood with a range of densities from 0.48-0.97 g/cm^3 was studied in both the axial and radial directions in the range of 1000-1450 ºC. From [104, 129].

Figure 20. Relative strength of several siliconized SiC ceramics including bioSiC, as a function of SiC volume fraction, at temperatures 1000 – 1300 ºC. The predictions from the minimum solid area models for several ideal microstructures are plotted as solid lines [102, 103]. The experimental values for several siliconized SiC materials including bioSiC are from [99].

Figure 21. Creep strain rates of bioSiC at 1175 ºC and 1600 ºC, at 250 MPa of applied stress. From [99].

Figure 22. Porous BioSiC candle prototypes used for hot-gas filtering experiments at 800ºC, from [113].

Tables

Table 1. Properties of carbon preforms and Si-infiltrated SiC materials from different types of wood [16, 18, 95]

		Balsa	*Pine*	*Oak*	*Maple*	*Beech*	*Ebony*	*Paulownia*	*MDF*
Pyrolysis weight loss (wt.%)		73.5	73.8	70.4	74.9	74.2	64.6	70.17	71.6
Pyrolysis shrinkage (%)	axial	21	23	17	20	22	14	20.06	24.75
	radial	22	28	28	30	32	25	20.81	23.95
	tangential	22	31	33	40	38	30	36.55	45.77
Density (g/cm^3)	Pyrolyzed	0.06	0.31	0.50	0.51	0.55	0.87	0.17	0.72
	Si-infiltrated	2.02	2.22	2.16	2.58	2.57	-	2.26	2.94
Porosity (%) (open/closed)	Pyrolyzed	22/70	21/57	30/40	43/22	42/21	23/20	75.81	42.65
	Si-infiltrated	11/14	11/14	8/5	3/5	3/2	3/-	14	3
Mean pore diameter (μm)*		40	20	170	35	30	-		
Si-content (wt%)		67	50	27	23	37	-	57	10

* Open pore channels free of Si.

Table 2. Microstructural features of pine-derived biomorphic SiC obtained by vapor infiltration of different precursors, from [60]

	Wood	Carbon template	Silicon carbide		
			SiO	Si	CH_3SiCl_3
Density ($g\ cm^{-3}$)					
Geometrical	0.47	0.35	0.6	1.0	1.2
Struts	1.4	1.4	2.5	3.1	3.1
Porosity (%)	67	76	80	70	60
Surface area ($m^2\ g^{-1}$)	-	46	16.1	3.3	0.5
Strut thickness (μm)	2	1.5	1	2	4
Biaxial strength (MPa)			4	13	21

Table 3. Room temperature mechanical properties of biomorphic SiC. σ_c and σ_f represent compressive and flexural strength respectively.

Wood	ρ (g·cm^{-3})	P (%)	Direction	σ_f (MPa)	σ_c (MPa)	E (MPa)	K_{IC} (MPa·m$^{1/2}$)	Ref.
Bamboo	2.38-2.51	51	Axial	120-180			1.75	[130]
Beech	2.50-2.61		Axial	180-200		250-290		[16]
	2.50-2.61		Radial	90-130		220-280		[16]
	2.10		Axial	228	438		2	[92]
	2.50		Axial	216	1080		3	[92]
	Porous	53-55	Axial		330-480	115-130	1.1-1.4	[97]
	Porous	52-55	Radial		24-24	10-27	0.5-0.7	[97]
Birch	2.71-2.77	9	Axial	210-320			2.4-4.3	[130]
Bubinga			Axial	186-240			2.4-2.8	[22]
Eucalyptus	2.60		Axial	226	1410		4.2	[92]
	2.63		Axial	290	1400	160-180	2.6-2.8	[91]
Mahogany	Porous	45-53	Axial		160-190	35-110	0.7-1.22	[97]
	Porous	46-50	Radial		57-75	15-21	0.46-0.6	[97]
	Porous	48-50	Tangential		31-35	12-20	-	[97]
			Axial	144		150-195	2	[21]
Maple	2.36		Axial	286-402		240-208	2.4-2.8	[21, 22]
MDF	2.68-2.72	<1	-	125-245			2.4-3.2	[130]
Pine	2.57-2.67	2	Axial	175-225			1.8-4.1	[130]
	2.25-2.30		Axial	125		180		[16]
	2.25-2.30		Radial	50-65		150-200		[16]
Poplar	Porous	59-64	Axial		135-250	30-76	0.8-1.1	[97]
	Porous	64-65	Radial		12	1	0-3	[97]
	Porous	58-60	Tangential		16-24	6-8	-	[97]
Red Oak	Porous	47-50	Axial		220-270	28-60	0.9-1.8	[97]
	Porous	44-46	Radial		8-18	5		[97]
	Porous	44-47	Tangential		5-28	8		[97]
	2.05-2.10		Axial	100-120		160-210		[16]
	2.05-2.10		Radial	30-60		150-200		[16]
Sapelly	Porous	54-59	Axial		50-127	15-22		[97]
	Porous	55-59	Radial		12-15	6-14		[97]
	Porous	54-57	Tangential		13-18	7-10		[97]

References

[1] A.R. Studart, U.T. Gonzenbach, E. Tervoort, L.J. Gauckler, Processing routes to macroporous ceramics: A review, J Am Ceram Soc 89(6) (2006) 1771-1789.

[2] J.-H. Eom, Y.-W. Kim, S. Raju, Processing and properties of macroporous silicon carbide ceramics: a review, Journal of Asian Ceramic Societies 1(3) (2013) 220-242.

[3] Y.M. Chiang, R.P. Messner, C. Terwilliger, D.R. Behrendt, Reaction-Formed Silicon-Carbide, Abstr Pap Am Chem S 200 (1990) 80-Ched.

[4] Y.M. Chiang, R.P. Messner, C.D. Terwilliger, D.R. Behrendt, Reaction-Formed Silicon-Carbide, Mat Sci Eng a-Struct 144 (1991) 63-74.

[5] M. Singh, D.R. Behrendt, Microstructure and Mechanical-Properties of Reaction-Formed Silicon-Carbide (Rfsc) Ceramics, Mat Sci Eng a-Struct 187(2) (1994) 183-187.

[6] M. Singh, D.R. Behrendt, Reactive Melt Infiltration of Silicon-Niobium Alloys in Microporous Carbons, J Mater Res 9(7) (1994) 1701-1708.

[7] M. Singh, D.R. Behrendt, Reactive Melt Infiltration of Silicon-Molybdenum Alloys into Microporous Carbon Preforms, Mat Sci Eng a-Struct 194(2) (1995) 193-200.

[8] M. Singh, T.A. Leonhardt, Microstructural characterization of reaction-formed silicon carbide ceramics, Mater Charact 35(4) (1995) 221-228.

[9] A. Wolfenden, P.J. Rynn, M. Singh, Measurement of Elastic and Anelastic Properties of Reaction-Formed Silicon Carbide-Based Materials, J Mater Sci 30(21) (1995) 5502-5507.

[10] M. Singh, R.M. Dickerson, Characterization of SiC fiber (SCS-6) reinforced-reaction-formed silicon carbide matrix composites, J Mater Res 11(3) (1996) 746-751.

[11] T.X. Fan, S.K. Chow, Z. Di, Biomorphic mineralization: From biology to materials, Prog Mater Sci 54(5) (2009) 542-659.

[12] T. Ota, M. Takahashi, T. Hibi, M. Ozawa, S. Suzuki, Y. Hikichi, H. Suzuki, Biomimetic process for producing SiC ''wood'', J Am Ceram Soc 78(12) (1995) 3409-3411.

[13] C.E. Byrne, D.C. Nagle, Carbonized wood monoliths - Characterization, Carbon 35(2) (1997) 267-273.

[14] C.E. Byrne, D.C. Nagle, Carbonization of wood for advanced materials applications, Carbon 35(2) (1997) 259-266.

[15] C.E. Byrne, D.C. Nagle, Cellulose derived composites - A new method for materials processing, Mater Res Innov 1(3) (1997) 137-144.

[16] P. Greil, T. Lifka, A. Kaindl, Biomorphic cellular silicon carbide ceramics from wood: II. Mechanical properties, J Eur Ceram Soc 18(14) (1998) 1975-1983.

[17] P. Greil, T. Lifka, A. Kaindl, Biomorphic cellular silicon carbide ceramics from wood: I. Processing and microstructure, J Eur Ceram Soc 18(14) (1998) 1961-1973.

[18] H. Sieber, C. Hoffmann, A. Kaindl, P. Greil, Biomorphic Cellular Ceramics, Adv Eng Mater 2(3) (2000) 105-109.

[19] P. Greil, Biomorphous ceramics from lignocellulosics, J Eur Ceram Soc 21(2) (2001) 105-118.

[20] M. Singh, Ecoceramics: Ceramics from wood, Adv Mater Process 160(3) (2002) 39-41.

[21] M. Singh, J.A. Salem, Mechanical properties and microstructure of biomorphic silicon carbide ceramics fabricated from wood precursors, J Eur Ceram Soc 22(14-15) (2002) 2709-2717.

[22] M. Singh, J. Martinez-Fernandez, A.R. de Arellano-Lopez, Environmentally conscious ceramics (ecoceramics) from natural wood precursors, Curr Opin Solid St M 7(3) (2003) 247-254.

[23] H. Sieber, M. Singh, Microcellular ceramics from wood, Cellular Ceramics: Structure, Manufacturing, Properties and Applications (2005) 122-136.

[24] A.R. de Arellano-Lopez, J. Martinez-Fernandez, P. Gonzalez, C. Dominguez, V. Fernandez-Quero, M. Singh, Biomorphic SiC: A new engineering ceramic material, Int J Appl Ceram Tec 1(1) (2004) 56-67.

[25] A.P. Scniewind, Concise Encyclopedia of Wood and Wood-based Materials, Pergamon Press, New York, 1989.

[26] A.J. Panshin, C. de Zeeuw, Textbook of Wood Technology, Mc Graw-Hill, New York, 1980.

[27] L.J. Gibson, M.F. Ashby, Cellular Solids: Structure and Properties, Pergamon Press1988.

[28] R.F. Evert, K. Esau, K. Esau, Esau's Plant anatomy : meristems, cells, and tissues of the plant body : their structure, function, and development, 3rd ed., Wiley-Interscience, Hoboken, N.J., 2006.

[29] J.M. Dinwoodie, Institute of Metals., Wood : nature's cellular, polymeric, fibre-composite, Institute of Metals, London ; Brookfield, VT, USA, 1989.

[30] R.H. Atalla, J.M. Hackney, Structural Polysaccharides in the Molecular Architecture of Plant Cell Walls, from Algae to Hardwoods, Materials Research Society Symposium 255 (1992) 399-405.

[31] H.P. Yang, R. Yan, H.P. Chen, D.H. Lee, C.G. Zheng, Characteristics of hemicellulose, cellulose and lignin pyrolysis, Fuel 86(12-13) (2007) 1781-1788.

[32] A.R. de Arellano-Lopez, J. Martinez Fernandez, F.M. Varela Feria, R.E. Sepulveda, M.J. Lopez Robledo, J. Llorca, J.Y. Pastor, M. Presas, K.T. Faber, V.S. Kaul, K.E. Pappacena, T.E. Wilkes, Processing, microstructure and mechanical behavior of SiC-based ceramics VIA naturally derived scaffolds, Ceramics Engineering and Science Proceedings 27 (2006) 635-650.

[33] P. Gonzalez, J.P. Borrajo, J. Serra, S. Chiussi, B. Leon, J. Martinez Fernandez, F.M. Varela Feria, A.R. de Arellano-Lopez, A. De Carlos, A. Munoz, M. Lopez, M. Singh, A new generation of bio-derived ceramic materials for medical applications, J. Biom. Mater. Res. A (2008).

[34] P. Greil, T. Lifka, A. Kaindl, Biomorphic Cellular Silicon Carbide Ceramics from Wood: I. Processing and Microstructure, J. Eur. Ceram. Soc. 18 (1998) 1961-1973.

[35] J. Martinez-Fernandez, A.R. de Arellano-Lopez, F.M. Varela-Feria, M. Singh, Procedimiento para la Fabricación de Carburo de Silicio a partir de Precursores Vegetales, Spain, 2001.

[36] J. Martinez-Fernandez, F.M. Varela-Feria, S. Lopez-Pombero, A.R. De Arellano-Lopez, M. Singh, Creep resistant biomorphic silicon-carbide based ceramics, Ceramics Engineering and Science Proceedings 22 (2001) 135-143.

[37] A. Muñoz, J. Martinez Fernandez, M. Singh, High temperature compressive mechanical behavior of joined biomorphic silicon carbide ceramics, J Eur Ceram Soc 22(14-15) (2002) 2727-2733.

[38] T. Ota, M. Takahashi, T. Hibi, M. Ozawa, S. Suzuki, Y. Hikichi, H. Suzuki, Biomimetic process for producing SiC 'wood', J. Am. Ceram. Soc. 78(12) (1995) 3409-3411.

[39] F.M. Varela-Feria, J. Ramirez-Rico, A.R. de Arellano-Lopez, J. Martinez-Fernandez, M. Singh, Reaction-formation mechanisms and microstructure evolution of biomorphic SiC, J Mater Sci 43(3) (2008) 933-941.

[40] F.M. Varela-Feria, J. Ramírez-Rico, J. Martínez-Fernández, A.R. De Arellano-López, M. Singh, Infiltration and reaction-formation mechanism and microstructural evolution of biomorphic SiC fabricated by Si-melt infiltration, Ceramic Transactions 177 (2006) 93-101.

[41] F.M. Varela Feria, Processing, Characterization and Mechanical Properties of Biomorphic Silicon Carbide, Condensed Matter Physics, Universidad de Sevilla, Sevilla, 2004.

[42] R.C.E. Weast, Handbook of Chemistry and Physics, 55th ed., CRC Press, Cleveland, OH, 1974.

[43] C. Zollfrank, H. Sieber, Microstructure evolution and reaction mechanism of biomorphous SiSiC ceramics, J Am Ceram Soc 88(1) (2005) 51-58.

[44] C. Zollfrank, H. Sieber, Microstructure and phase morphology of wood derived biomorphous SiSiC-ceramics, J Eur Ceram Soc 24(2) (2004) 495-506.

[45] M.H. Hon, R.F. Davis, Self-Diffusion of C-14 in Polycrystalline Beta-SiC, J Mater Sci 14(10) (1979) 2411-2421.

[46] R. Pampuch, J. Bialoskorski, E. Walasek, Mechanism of Reactions in the Sii + Cf System and the Self-Propagating High-Temperature Synthesis of Silicon-Carbide, Ceram Int 13(1) (1987) 63-68.

[47] R. Pampuch, E. Walasek, J. Bialoskorski, Reaction-Mechanism in Carbon Liquid Silicon Systems at Elevated-Temperatures, Ceram Int 12(2) (1986) 99-106.

[48] M.H. Hon, R.F. Davis, D.E. Newbury, Self-Diffusion of Si-30 in Polycrystalline Beta-SiC, J Mater Sci 15(8) (1980) 2073-2080.

[49] C. Torres-Raya, D. Hernandez-Maldonado, J. Ramirez-Rico, C. Garcia-Ganan, A.R. de Arellano-Lopez, J. Martinez-Fernandez, Fabrication, chemical etching, and compressive

strength of porous biomimetic SiC for medical implants, J Mater Res 23(12) (2008) 3247-3254.

[50] J. Ramirez-Rico, C. Torres-Raya, D. Hernandez-Maldonado, C. Garcia-Gañan, J. Martinez-Fernandez, A.R. De Arellano-López, Porous biomorphic SiC for medical implants processed from natural and artificial precursors, Ceramic Engineering and Science Proceedings, 2010, pp. 203-214.

[51] K.E. Pappacena, S.P. Gentry, T.E. Wilkes, M.T. Johnson, S. Xie, A. Davis, K.T. Faber, Effect of pyrolyzation temperature on wood-derived carbon and silicon carbide, J Eur Ceram Soc 29(14) (2009) 3069-3077.

[52] T.E. Wilkes, S.R. Stock, F. De Carlo, X. Xiao, K.T. Faber, X-ray micro-computed tomography of beech wood and biomorphic C, SiC and Al/SiC composites, Philos Mag 89(17) (2009) 1373-1389.

[53] E. Vogli, H. Sieber, P. Greil, Biomorphic SiC-ceramic prepared by Si-vapor phase infiltration of wood, J Eur Ceram Soc 22(14-15) (2002) 2663-2668.

[54] E. Vogli, J. Mukerji, C. Hoffman, R. Kladny, H. Sieber, P. Greil, Conversion of oak to cellular silicon carbide ceramic by gas-phase reaction with silicon monoxide, J Am Ceram Soc 84(6) (2001) 1236-1240.

[55] J.M. Qian, J.P. Wang, G.Y. Hou, G.J. Qiao, Z.H. Jin, Preparation and characterization of biomorphic SiC hollow fibers from wood by chemical vapor infiltration, Scripta Mater 53(12) (2005) 1363-1368.

[56] J.W. Kim, S.W. Myoung, H.C. Kim, J.H. Lee, Y.G. Jung, C.Y. Jo, Synthesis of SiC microtubes with radial morphology using biomorphic carbon template, Mat Sci Eng a-Struct 434(1-2) (2006) 171-177.

[57] D.A. Streitwieser, N. Popovska, H. Gerhard, Optimization of the ceramization process for the production of three-dimensional biomorphic porous SiC ceramics by chemical vapor infiltration (CVI), J Eur Ceram Soc 26(12) (2006) 2381-2387.

[58] D.A. Streitwieser, N. Popovska, H. Gerhard, G. Emig, Application of the chemical vapor infiltration and reaction (M-R) technique for the preparation of highly porous biomorphic SiC ceramics derived from paper, J Eur Ceram Soc 25(6) (2005) 817-828.

[59] H. Ghanem, E. Alkhateeb, H. Gerhard, N. Popovska, Oxidation behavior of silicon carbide based biomorphic ceramics prepared by chemical vapor infiltration and reaction technique, Ceram Int 35(7) (2009) 2767-2774.

[60] P. Greil, E. Vogli, T. Fey, A. Bezold, N. Popovska, H. Gerhard, H. Sieber, Effect of microstructure on the fracture behavior of biomorphous silicon carbide ceramics, J Eur Ceram Soc 22(14-15) (2002) 2697-2707.

[61] H. Sieber, C. Zollfrank, N. Popovska, D. Almeida, H. Gerhard, Gas phase processing of porous, biomorphous TiC-ceramics, Euro Ceramics Viii, Pts 1-3 264-268 (2004) 2227-2230.

[62] N. Popovska, D. Almeida-Streitwieser, C. Xu, H. Gerhard, H. Sieber, Kinetic analysis of the processing of porous biomorphic titanium carbide ceramics by chemical vapor infiltration, Chem Vapor Depos 11(3) (2005) 153-158.

[63] M. Kormann, H. Gerhard, N. Popovska, Comparative study of carbide-derived carbons obtained from biomorphic TiC and SiC structures, Carbon 47(1) (2009) 242-250.

[64] J.M. Qian, J.P. Wang, Z.H. Jin, Preparation of biomorphic SiC ceramic by carbothermal reduction of oak wood charcoal, Mat Sci Eng a-Struct 371(1-2) (2004) 229-235.

[65] Y.S. Shin, C.M. Wang, G.L. Exarhos, Synthesis of SiC ceramics by the carbothermal reduction of mineralized wood with silica, Adv Mater 17(1) (2005) 73-+.

[66] J.M. Qian, Z.H. Jin, Preparation and characterization of porous, biomorphic SiC ceramic with hybrid pore structure, J Eur Ceram Soc 26(8) (2006) 1311-1316.

[67] T.L.Y. Cheung, D.H.L. Ng, Conversion of bamboo to biomorphic composites containing silica and silicon carbide nanowires, J Am Ceram Soc 90(2) (2007) 559-564.

[68] J. Locs, L. Berzina-Cimdina, A. Zhurinsh, D. Loca, Optimized vacuum/pressure sol impregnation processing of wood for the synthesis of porous, biomorphic SiC ceramics, J Eur Ceram Soc 29(8) (2009) 1513-1519.

[69] S.M. Manocha, H. Patel, L.M. Manocha, Effect of Steam Activation on Development of Light Weight Biomorphic Porous SiC from Pine Wood Precursor, J Mater Eng Perform 22(2) (2013) 396-404.

[70] A. Herzog, R. Klingner, U. Vogt, T. Graule, Wood-derived porous SiC ceramics by sol infiltration and carbothermal reduction, J Am Ceram Soc 87(5) (2004) 784-793.

[71] C.R. Rambo, J. Cao, O. Rusina, H. Sieber, Manufacturing of biomorphic (Si, Ti, Zr)-carbide ceramics by sol-gel processing, Carbon 43(6) (2005) 1174-1183.

[72] C.R. Rambo, J. Cao, H. Sieber, Biomorphic (Si, Ti, Zr) - Carbide synthesized through sol-gel process, Innovative Processing and Synthesis of Ceramics, Glasses and Composites Viii 166 (2005) 49-55.

[73] T. Ota, M. Imaeda, H. Takase, M. Kobayashi, N. Kinoshita, T. Hirashita, H. Miyazaki, Y. Hikichi, Porous titania ceramic prepared by mimicking silicified wood, J Am Ceram Soc 83(6) (2000) 1521-1523.

[74] M. Mizutani, H. Takase, N. Adachi, T. Ota, K. Daimon, Y. Hikichi, Porous ceramics prepared by mimicking silicified wood, Sci Technol Adv Mat 6(1) (2005) 76-83.

[75] M. Singh, B.M. Yee, Reactive processing of environmentally conscious, biomorphic ceramics from natural wood precursors, J Eur Ceram Soc 24(2) (2004) 209-217.

[76] C.R. Rambo, J. Cao, H. Sieber, Preparation and properties of highly porous, biomorphic YSZ ceramics, Mater Chem Phys 87(2-3) (2004) 345-352.

[77] J. Cao, C.R. Rambo, H. Sieber, Preparation of porous Al2O3-Ceramics by biotemplating of wood, J Porous Mat 11(3) (2004) 163-172.

[78] J. Cao, C.R. Rambo, H. Sieber, Manufacturing of microcellular, biomorphous oxide ceramics from native pine wood, Ceram Int 30(7) (2004) 1967-1970.

[79] H. Sieber, C. Rambo, J. Cao, E. Vogli, P. Greil, Manufacturing of porous oxide ceramics by replication of plant morphologies, Euro Ceramics Vii, Pt 1-3 206-2 (2002) 2009-2012.

[80] G. Filardo, E. Kon, A. Tampieri, R. Cabezas-Rodriguez, A. Di Martino, M. Fini, G. Giavaresi, M. Lelli, J. Martinez-Fernandez, L. Martini, J. Ramirez-Rico, F. Salamanna, M. Sandri, S. Sprio, M. Marcacci, New Bio-Ceramization Processes Applied to Vegetable Hierarchical Structures for Bone Regeneration: An Experimental Model in Sheep, Tissue Eng Pt A 20(3-4) (2014) 763-773.

[81] A. Ruffini, S. Sprio, A. Tampieri, Study of the hydrothermal transformation of wood-derived calcium carbonate into 3D hierarchically organized hydroxyapatite, Chem Eng J 217 (2013) 150-158.

[82] A. Tampieri, S. Sprio, A. Ruffini, G. Celotti, I.G. Lesci, N. Roveri, From wood to bone: multi-step process to convert wood hierarchical structures into biomimetic hydroxyapatite scaffolds for bone tissue engineering, J Mater Chem 19(28) (2009) 4973-4980.

[83] C. Zollfrank, N. Travitzky, H. Sieber, T. Selchert, P. Greil, Biomorphous SiSiC/Al-Si ceramic composites manufactured by squeeze casting: Microstructure and mechanical properties, Adv Eng Mater 7(8) (2005) 743-746.

[84] A. Herzog, U.F. Vogt, S. Siegmann, O. Beffort, Aluminium metal matrix composites based on biomorphic silicon carbide, Adv Eng Mater 8(10) (2006) 980-983.

[85] T.E. Wilkes, M.L. Young, R.E. Sepulveda, D.C. Dunand, K.T. Faber, Composites by aluminum infiltration of porous silicon carbide derived from wood precursors, Scripta Mater 55(12) (2006) 1083-1086.

[86] T.E. Wilkes, J.Y. Pastor, J. Llorca, K.T. Faber, Mechanical properties of wood-derived silicon carbide aluminum-alloy composites as a function of temperature, J Mater Res 23(6) (2008) 1732-1743.

[87] T.E. Wilkes, B.J. Harder, J.D. Almer, K.T. Faber, Load partitioning in honeycomb-like silicon carbide aluminum alloy composites, Acta Mater 57(20) (2009) 6234-6242.

[88] K.E. Pappacena, M.T. Johnson, H. Wang, W.D. Porter, K.T. Faber, Thermal properties of wood-derived copper-silicon carbide composites fabricated via electrodeposition, Compos Sci Technol 70(3) (2010) 478-484.

[89] K.E. Pappacena, M.T. Johnson, S. Xie, K.T. Faber, Processing of wood-derived copper-silicon carbide composites via electrodeposition, Compos Sci Technol 70(3) (2010) 485-491.

[90] F. Gutierrez-Mora, K.C. Goretta, F.M. Varela-Feria, A.R.A. Lopez, J.M. Fernandez, Indentation hardness of biomorphic SiC, Int J Refract Met H 23(4-6) (2005) 369-374.

[91] M. Presas, J.Y. Pastor, J. Llorca, A.R.A. Lopez, J.M. Fernandez, R. Sepulveda, Microstructure and fracture properties of biomorphic SiC, Int J Refract Met H 24(1-2) (2006) 49-54.

[92] M. Presas, J.Y. Pastor, J. Llorca, A.R. de Arellano-Lopez, J. Martinez-Fernandez, R.E. Sepulveda, Mechanical behavior of biomorphic Si/SiC porous composites, Scripta Mater 53(10) (2005) 1175-1180.

[93] M. Presas, J.Y. Pastor, J. Llorca, A.R. De Arellano-Lopez, J. Martinez-Fernandez, R. Sepulveda, Microestructure and mechanical properties of biomorphic SiC obtained from eucalyptus, Bol Soc Esp Ceram V 44(6) (2005) 363-367.

[94] D.J. Lee, J.J. Jang, H.S. Park, Y.C. Kim, K.H. Lim, S.B. Park, S.H. Hong, Fabrication of biomorphic SiC composites using wood preforms with different structures, Ceram Int 38(4) (2012) 3089-3095.

[95] H.S. Park, J.J. Jang, K.H. Lee, K.H. Lim, S.B. Park, Y.C. Kim, S.H. Hong, Effects of microstructure on flexural strength of biomorphic C/SiC composites, Int J Fracture 151(2) (2008) 233-245.

[96] G.Y. Hou, Z.H. Jin, J.M. Qian, Effect of holding time on the basic properties of biomorphic SiC ceramic derived from beech wood, Mat Sci Eng a-Struct 452 (2007) 278-283.

[97] V.S. Kaul, K.T. Faber, R. Sepulveda, A.R.D. Lopez, J. Martinez-Fernandez, Precursor selection and its role in the mechanical properties of porous SiC derived from wood, Mat Sci Eng a-Struct 428(1-2) (2006) 225-232.

[98] V.S. Kaul, K.T. Faber, Nanoindentation analysis of the elastic properties of porous SiC derived from wood, Scripta Mater 58(10) (2008) 886-889.

[99] J. Martinez-Fernandez, A. Munoz, A.R.D. Lopez, F.M.V. Feria, A. Dominguez-Rodriguez, M. Singh, Microstructure-mechanical properties correlation in siliconized silicon carbide ceramics, Acta Mater 51(11) (2003) 3259-3275.

[100] A. Munoz, J. Martinez-Fernandez, A. Dominguez-Rodriguez, M. Singh, High-temperature compressive strength of reaction-formed silicon carbide (RFSC) ceramics, J Eur Ceram Soc 18(1) (1998) 65-68.

[101] P. Sangsuwan, J.A. Orejas, J.E. Gatica, S.N. Tewari, M. Singh, Reaction-bonded silicon carbide by reactive infiltration, Ind Eng Chem Res 40(23) (2001) 5191-5198.

[102] R.W. Rice, Comparison of physical property porosity behaviour with minimum solid area models, J Mater Sci 31(6) (1996) 1509-1528.

[103] R.W. Rice, Evaluation and extension of physical property-porosity models based on minimum solid area, J Mater Sci 31(1) (1996) 102-118.

[104] F.M. Varela-Feria, J. Martinez-Fernandez, A.R. de Arellano-Lopez, M. Singh, Low density biomorphic silicon carbide: microstructure and mechanical properties, J Eur Ceram Soc 22(14-15) (2002) 2719-2725.

[105] A.R. de Arellano-Lopez, J. Martinez-Fernandez, F.M. Varela-Feria, T.S. Orlova, K.C. Goretta, F. Gutierrez-Mora, N. Chen, J.L. Routbort, Erosion and strength degradation of biomorphic SiC, J Eur Ceram Soc 24(5) (2004) 861-870.

[106] Q. Wang, W.Z. Sun, G.Q. Jin, Y.Y. Wang, X.Y. Guo, Biomorphic SiC pellets as catalyst support for partial oxidation of methane to syngas, Appl Catal B-Environ 79(4) (2008) 307-312.

[107] T.L. Church, S. Fallani, J. Liu, M. Zhao, A.T. Harris, Novel biomorphic Ni/SiC catalysts that enhance cellulose conversion to hydrogen, Catal Today 190(1) (2012) 98-106.

[108] G.M. Arzac, J. Ramirez-Rico, A. Gutierrez-Pardo, M.C.J. de Haro, D. Hufschmidt, J. Martinez-Fernandez, A. Fernandez, Monolithic supports based on biomorphic SiC for the catalytic combustion of hydrogen, Rsc Adv 6(71) (2016) 66373-66384.

[109] A. Zampieri, H. Sieber, T. Selvam, G.T.P. Mabande, W. Schwieger, F. Scheffler, M. Scheffler, P. Greil, Biomorphic cellular SiSiC/zeolite ceramic composites: From Rattan palm to bioinspired structured monoliths for catalysis and sorption, Adv Mater 17(3) (2005) 344-+.

[110] Y.Y. Wang, G.Q. Jin, X.Y. Guo, Growth of ZSM-5 coating on biomorphic porous silicon carbide derived from durra, Micropor Mesopor Mat 118(1-3) (2009) 302-306.

[111] A. Gomez-Martin, M.P. Orihuela, J.A. Becerra, J. Martinez-Fernandez, J. Ramirez-Rico, Permeability and mechanical integrity of porous biomorphic SiC ceramics for application as hot-gas filters, Mater Design 107 (2016) 450-460.

[112] M.A. Bautista, J.Q. Cancapa, J.M. Fernandez, M.A. Rodriguez, M. Singh, Microstructural and mechanical evaluation of porous biomorphic silicon carbide for high temperature filtering applications, J Eur Ceram Soc 31(7) (2011) 1325-1332.

[113] B. Alonso-Farinas, M. Lupion, M. Rodriguez-Galan, J. Martinez-Fernandez, New candle prototype for hot gas filtration industrial applications, Fuel 114 (2013) 120-127.

[114] P. Gonzalez, J.P. Borrajo, J. Serra, S. Chiussi, B. Leon, J. Martinez-Fernandez, F.M. Varela-Feria, A.R. de Arellano-Lopez, A. de Carlos, F.M. Munoz, M. Lopez, M. Singh, A new generation of bio-derived ceramic materials for medical applications, J Biomed Mater Res A 88A(3) (2009) 807-813.

[115] J.P. Borrajo, J. Serra, S. Liste, R. Gonzalez, S. Chiussi, B. Leon, M. Perez-Amor, Pulsed laser deposition of hydroxylapatite thin films on biomorphic silicon carbide ceramics, Appl Surf Sci 248(1-4) (2005) 355-359.

[116] J.P. Borrajo, P. Gonzalez, J. Serra, S. Liste, S. Chiussi, B. Leon, A. De Carlos, F.M. Varela-Feria, J. Martinez-Fernandez, A.R. De Arellano-Lopez, Cytotoxicity study of biomorphic SiC ceramics coated with bioactive glass., Bol Soc Esp Ceram V 45(2) (2006) 109-114.

[117] J.P. Borrajo, P. Gonzalez, J. Serra, S. Liste, S. Chiussi, B. Leon, A. de Carlos, F.M. Varela-Feria, J. Martinez-Fernandez, A.R. de Arellano-Lopez, Biomorphic silicon carbide ceramics coated with bioactive glass for medical applications, Mater Sci Forum 514-516 (2006) 970-974.

[118] P. Gonzalez, J. Serra, S. Liste, S. Chiussi, B. Leon, M. Perez-Amor, J. Martinez-Fernandez, A.R. de Arellano-Lopez, F.M. Varela-Feria, New biomorphic SiC ceramics coated with bioactive glass for biomedical applications, Biomaterials 24(26) (2003) 4827-4832.

[119] J. Will, A. Hoppe, F.A. Muller, C.T. Raya, J.M. Fernandez, P. Greil, Bioactivation of biomorphous silicon carbide bone implants, Acta Biomater 6(12) (2010) 4488-4494.

[120] M. Lelli, I. Foltran, E. Foresti, J. Martinez-Fernandez, C. Torres-Raya, F.M. Varela-Feria, N. Roveri, Biomorphic Silicon Carbide Coated with an Electrodeposition of Nanostructured Hydroxyapatite/Collagen as Biomimetic Bone Filler and Scaffold, Adv Eng Mater 12(8) (2010) B348-B355.

[121] S.L. Candelaria, Y.Y. Shao, W. Zhou, X.L. Li, J. Xiao, J.G. Zhang, Y. Wang, J. Liu, J.H. Li, G.Z. Cao, Nanostructured carbon for energy storage and conversion, Nano Energy 1(2) (2012) 195-220.

[122] L.L. Zhang, X.S. Zhao, Carbon-based materials as supercapacitor electrodes, Chem Soc Rev 38(9) (2009) 2520-2531.

[123] P. Simon, Y. Gogotsi, Materials for electrochemical capacitors, Nat Mater 7(11) (2008) 845-854.

[124] M. Kaarik, M. Arulepp, M. Karelson, J. Leis, The effect of graphitization catalyst on the structure and porosity of SiC derived carbons, Carbon 46(12) (2008) 1579-1587.

[125] T. Fey, B. Zierath, A.M. Kern, P. Greil, B.J.M. Etzold, An advanced method to manufacture hierarchically structured carbide-derived carbon monoliths, Carbon 70 (2014) 30-37.

[126] M. Schmirler, T. Knorr, T. Fey, A. Lynen, P. Greil, B.J.M. Etzold, Fast production of monolithic carbide-derived carbons with secondary porosity produced by chlorination of carbides containing a free metal phase, Carbon 49(13) (2011) 4359-4367.

[127] M. Adam, M. Oschatz, W. Nickel, S. Kaskel, Preparation of hierarchical porous biomorphic carbide-derived carbon by polycarbosilane impregnation of wood, Micropor Mesopor Mat 210 (2015) 26-31.

[128] M. Kormann, H. Ghanem, H. Gerhard, N. Popovska, Processing of carbide-derived carbon (CDC) using biomorphic porous titanium carbide ceramics, J Eur Ceram Soc 28(6) (2008) 1297-1303.

[129] J. Martínez-Fernández, F.M. Valera-Feria, M. Singh, Microstructure and Thermomechanical Characterization of Biomorphic Silicon Carbide Based Ceramics, Scripta Mater 43 (2000) 813-818.

[130] G.J. Qiao, R. Ma, N. Cai, C.G. Zhang, Z.H. Jin, Mechanical properties and microstructure of Si/SiC materials derived from native wood, Mat Sci Eng a-Struct 323(1-2) (2002) 301-305.

FIGURE 1

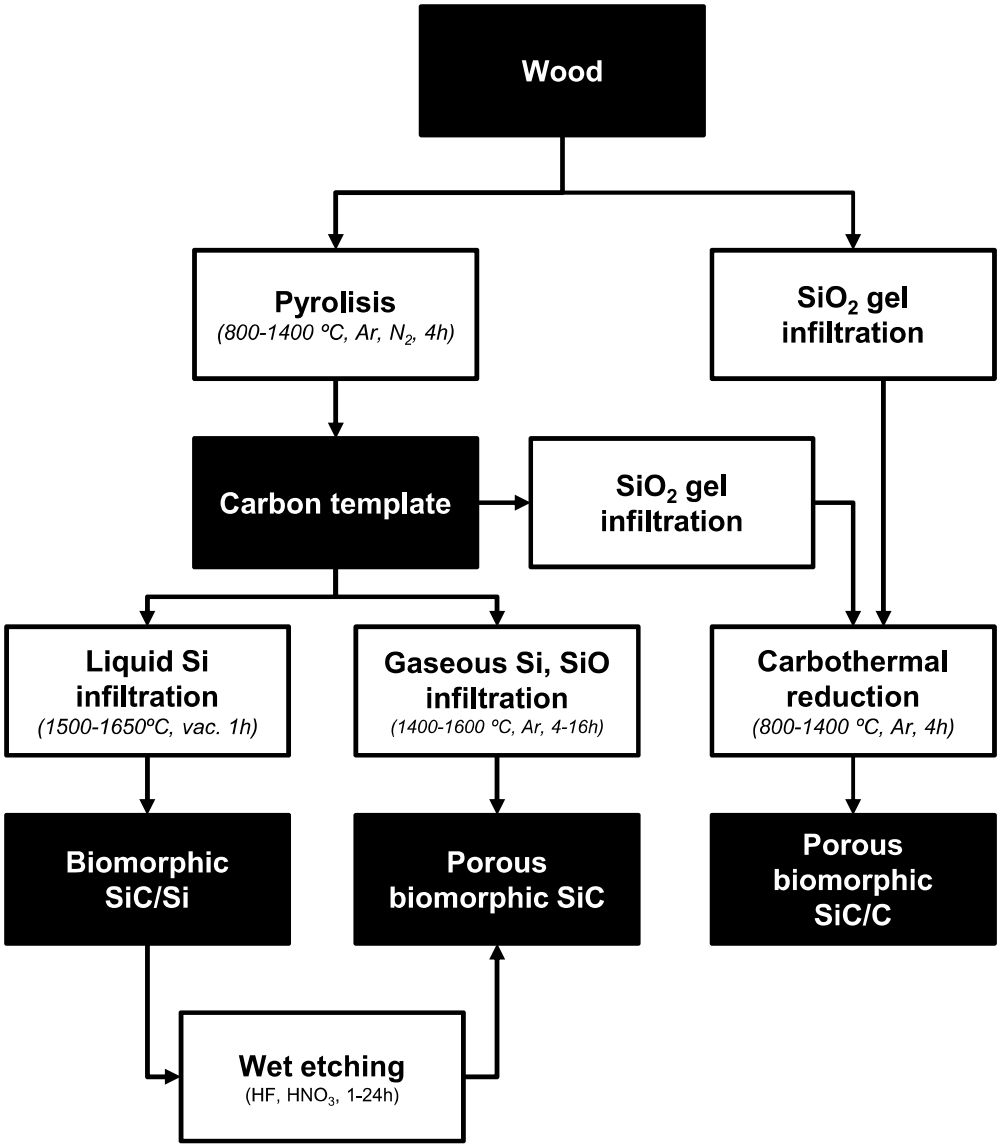
Wood
Pyrolisis
(800-1400 ºC, Ar, N2, 4h)
SiO2 gel infiltration
Carbon template
SiO2 gel infiltration
Liquid Si infiltration
(1500-1650ºC, vac. 1h)
Gaseous Si, SiO infiltration
(1400-1600 ºC, Ar, 4-16h)
Carbothermal reduction
(800-1400 ºC, Ar, 4h)
Biomorphic SiC/Si
Porous biomorphic SiC
Porous biomorphic SiC/C
Wet etching
(HF, HNO3, 1-24h)

FIGURE 2

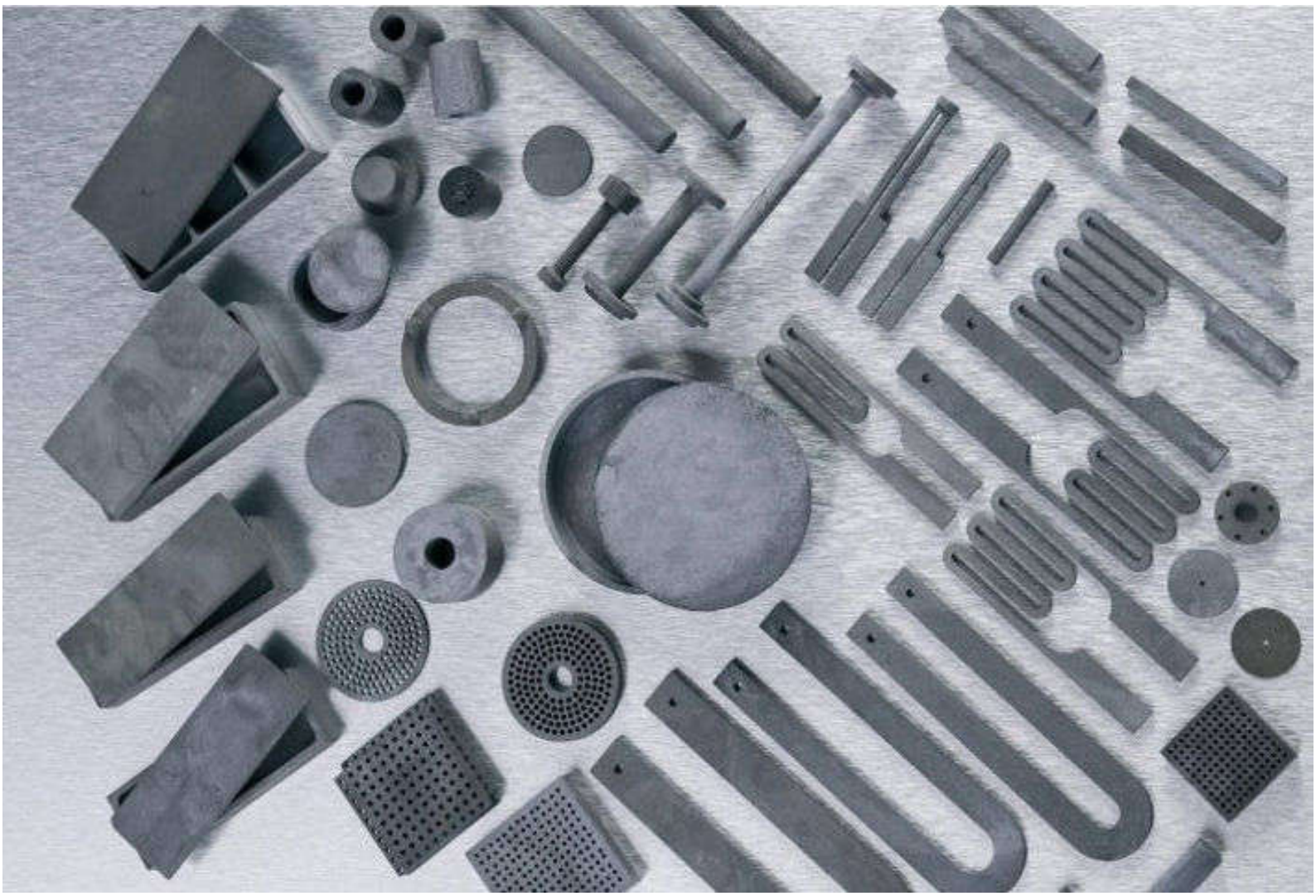

FIGURE 3

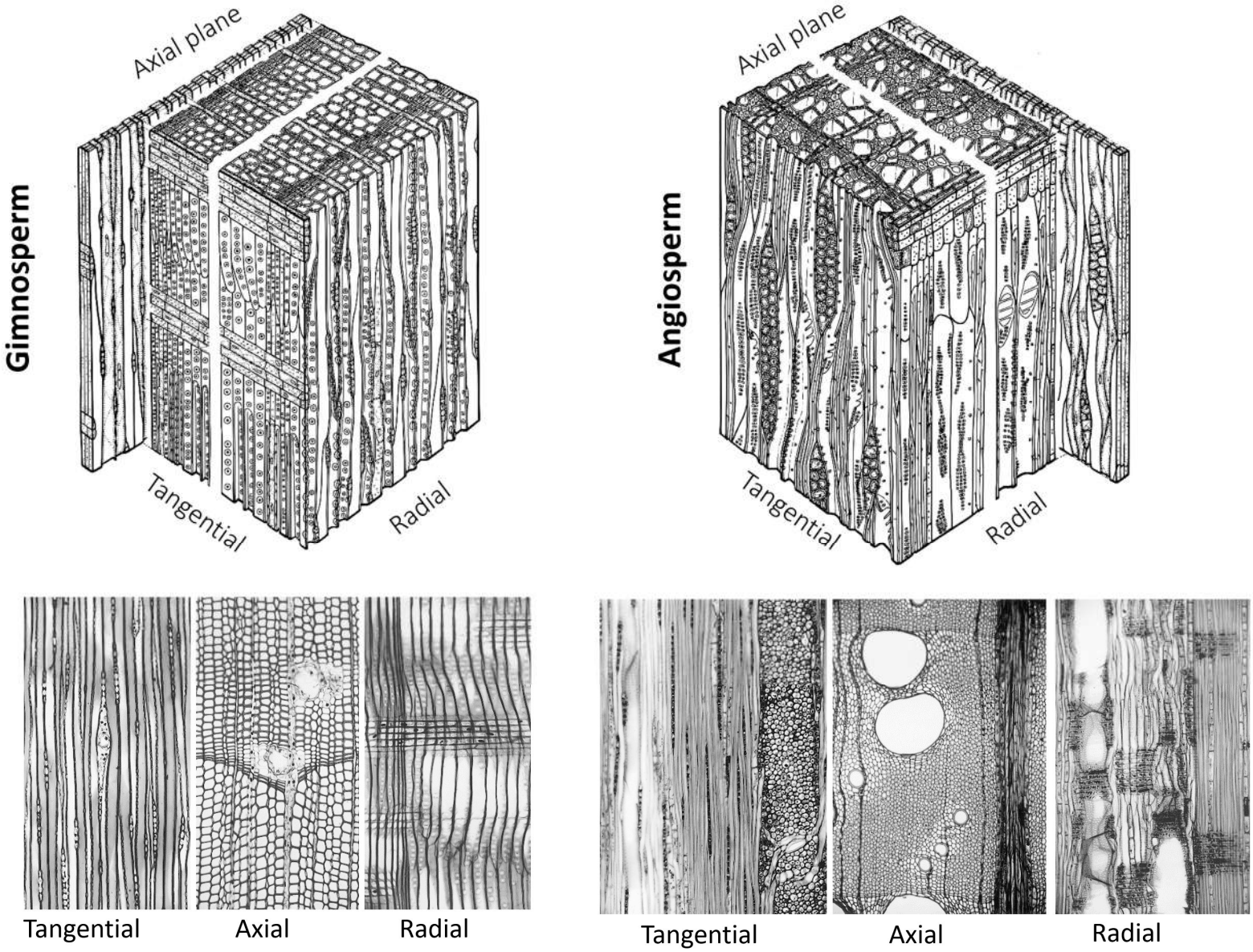
Gimnosperm
Axial plane
Tangential
Radial
Angiosperm
Axial plane
Tangential
Radial
Tangential
Axial
Radial
Tangential
Axial
Radial

FIGURE 4

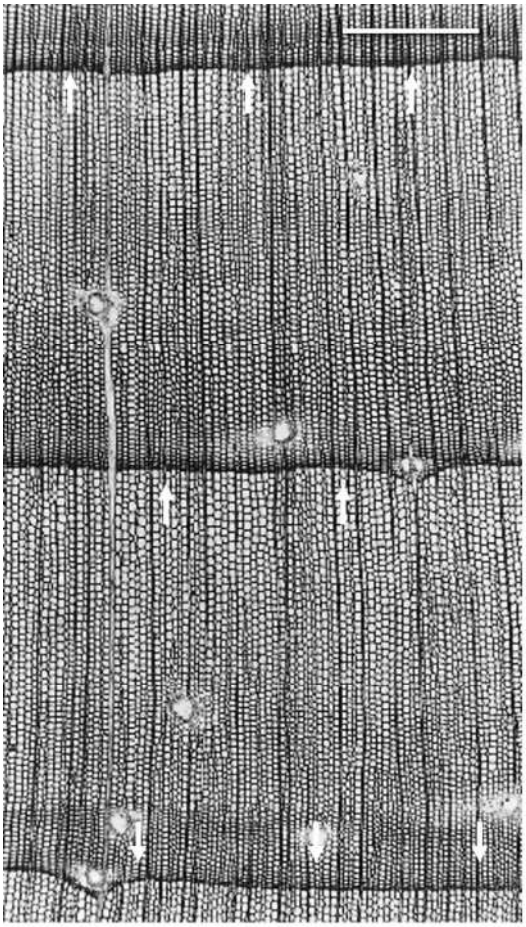

Non-porous
White pine (*Pinus strobus*)

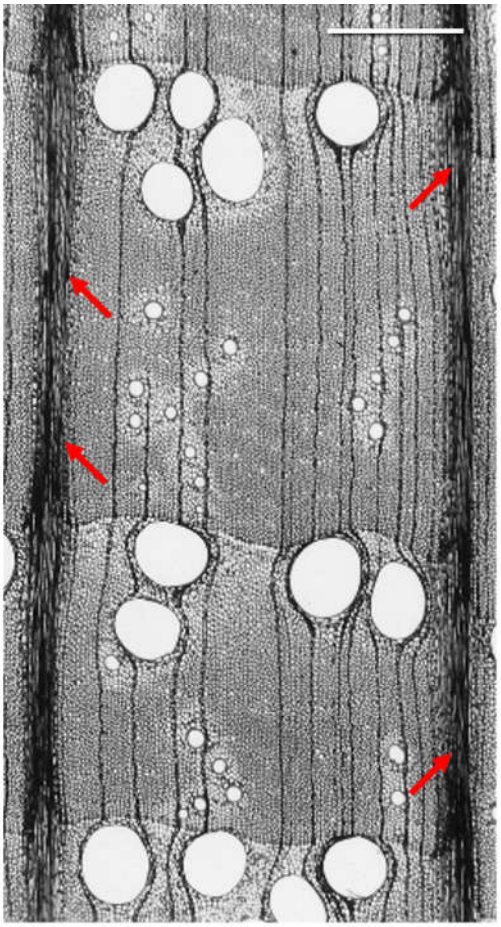

Ring-porous
Red oak (*Quercus rubra*)

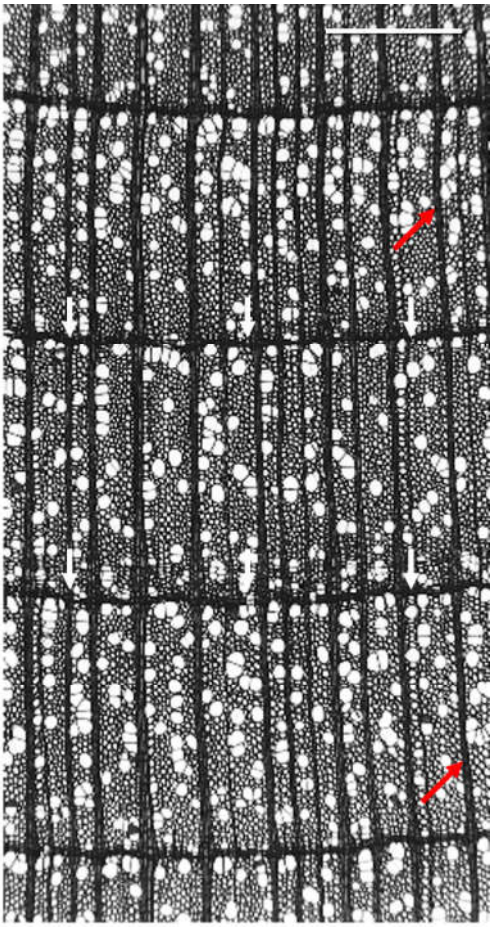

Diffuse-porous
Tulip tree (*Liriodendron tulipifera*)

FIGURE 5

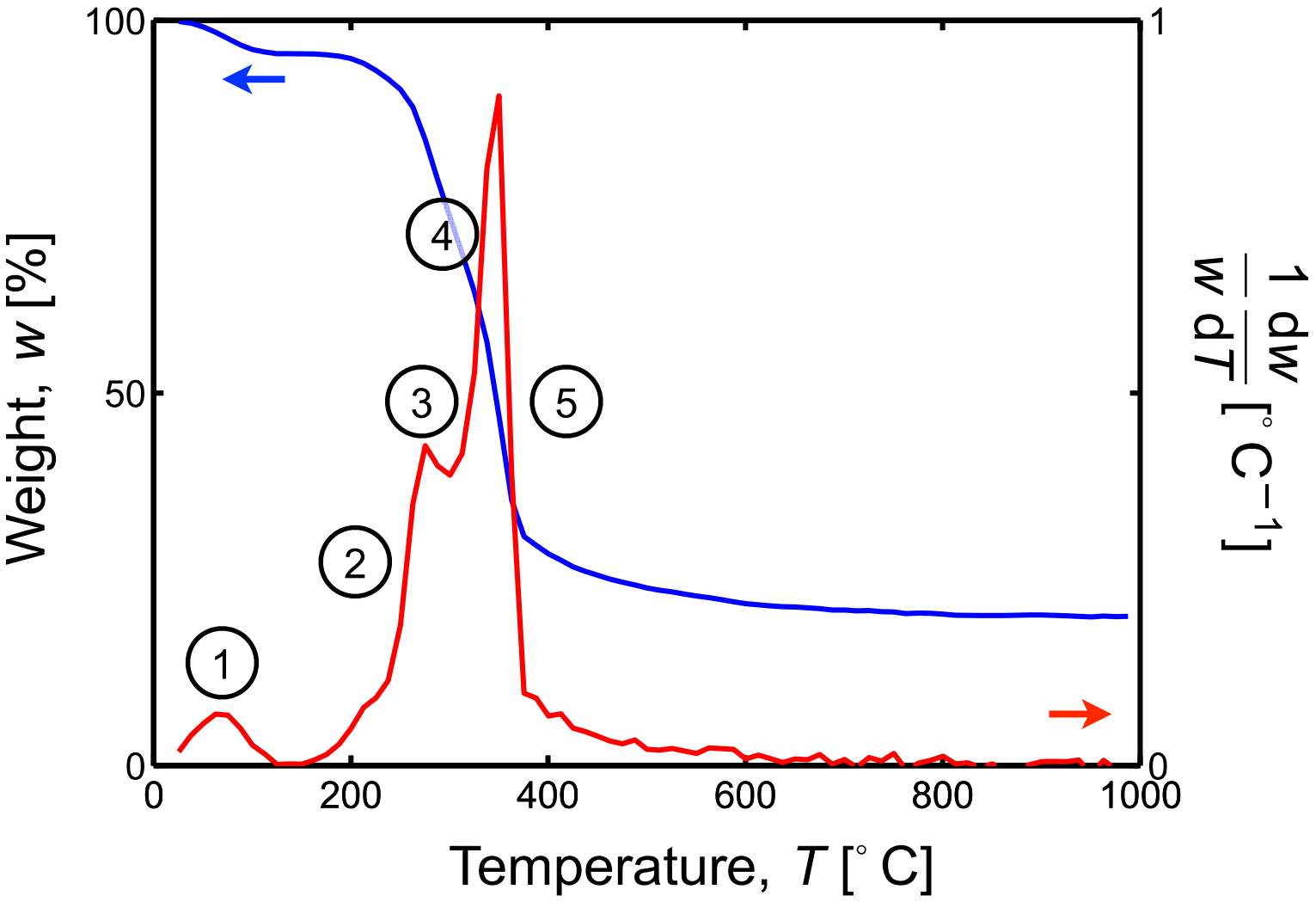
100
50
0
1
0
0
200
400
600
800
1000
Weight, w [%]
1 dw / w dT [°C−1]
Temperature, T [°C]
1
2
3
4
5

FIGURE 6

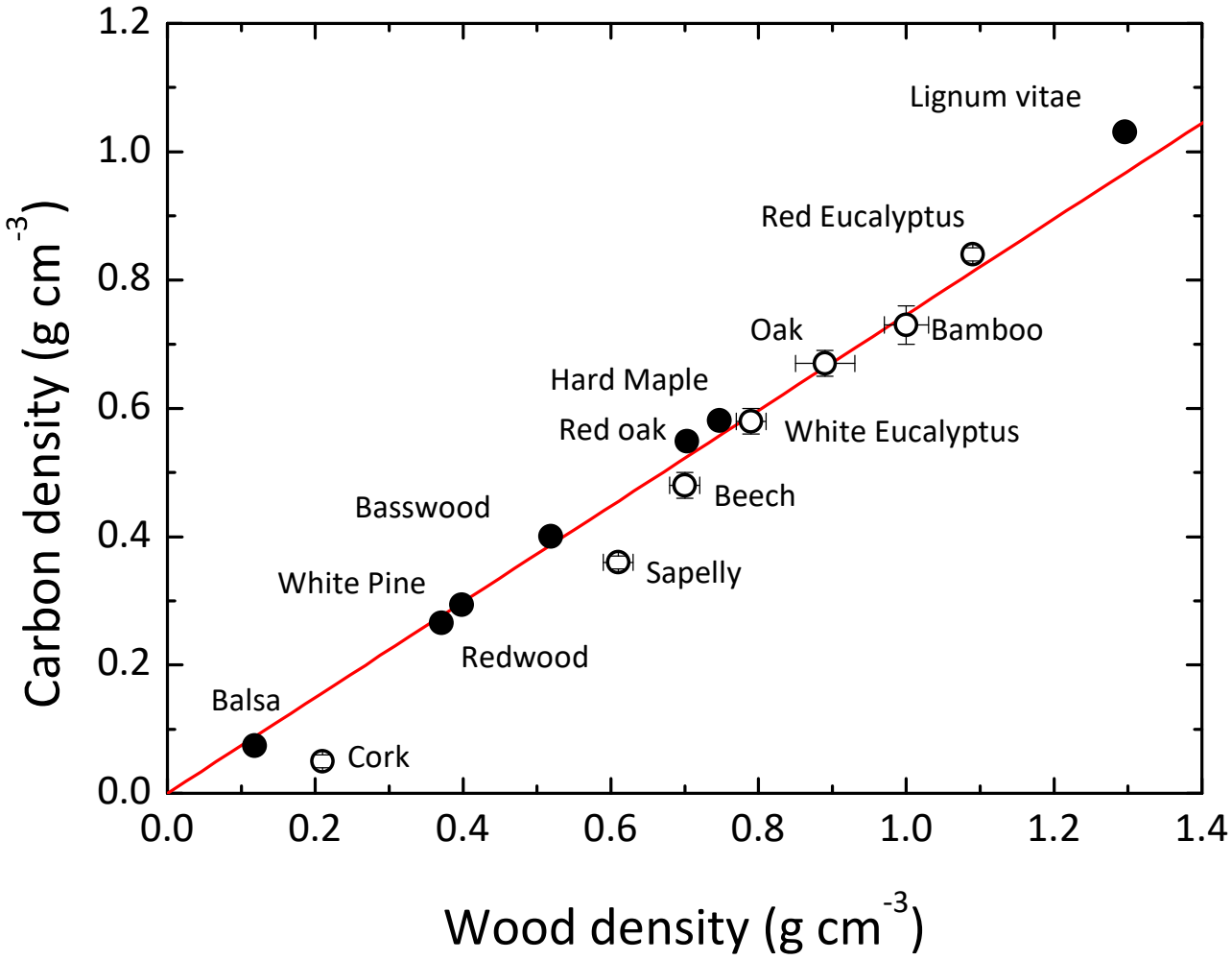
Carbon density (g cm-3)
Wood density (g cm-3)
0.0
0.2
0.4
0.6
0.8
1.0
1.2
1.4
Lignum vitae
Red Eucalyptus
Oak
Bamboo
Hard Maple
Red oak
White Eucalyptus
Beech
Basswood
Sapelly
White Pine
Redwood
Balsa
Cork

FIGURE 7

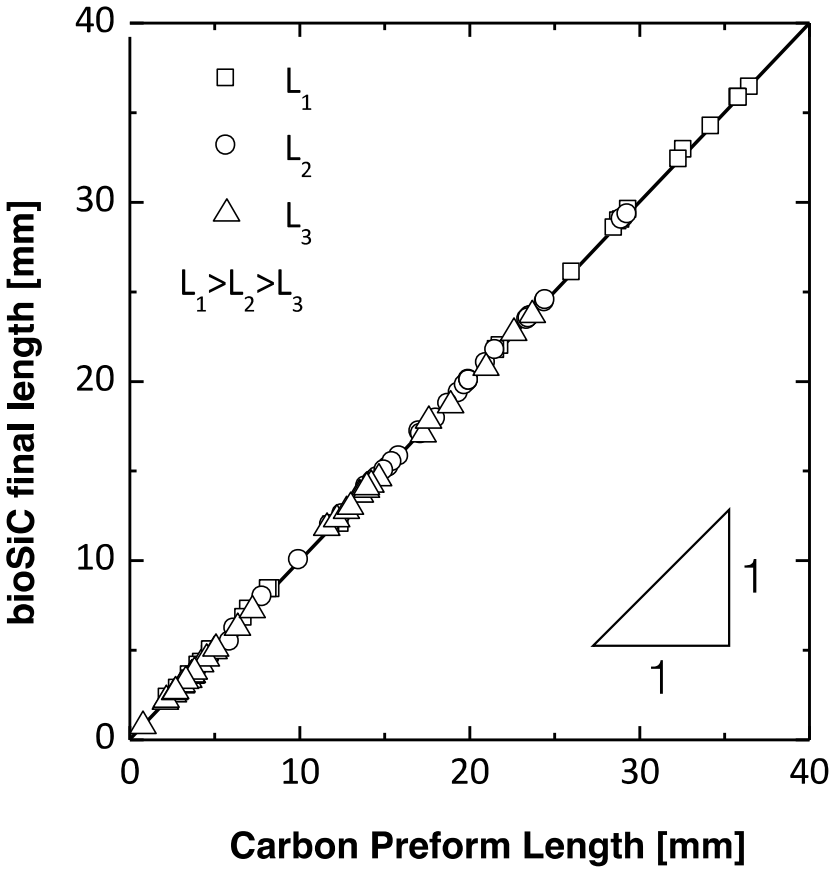
40
30
20
10
0
0
10
20
30
40
L1
L2
L3
L1>L2>L3
1
1
bioSiC final length [mm]
Carbon Preform Length [mm]

FIGURE 8

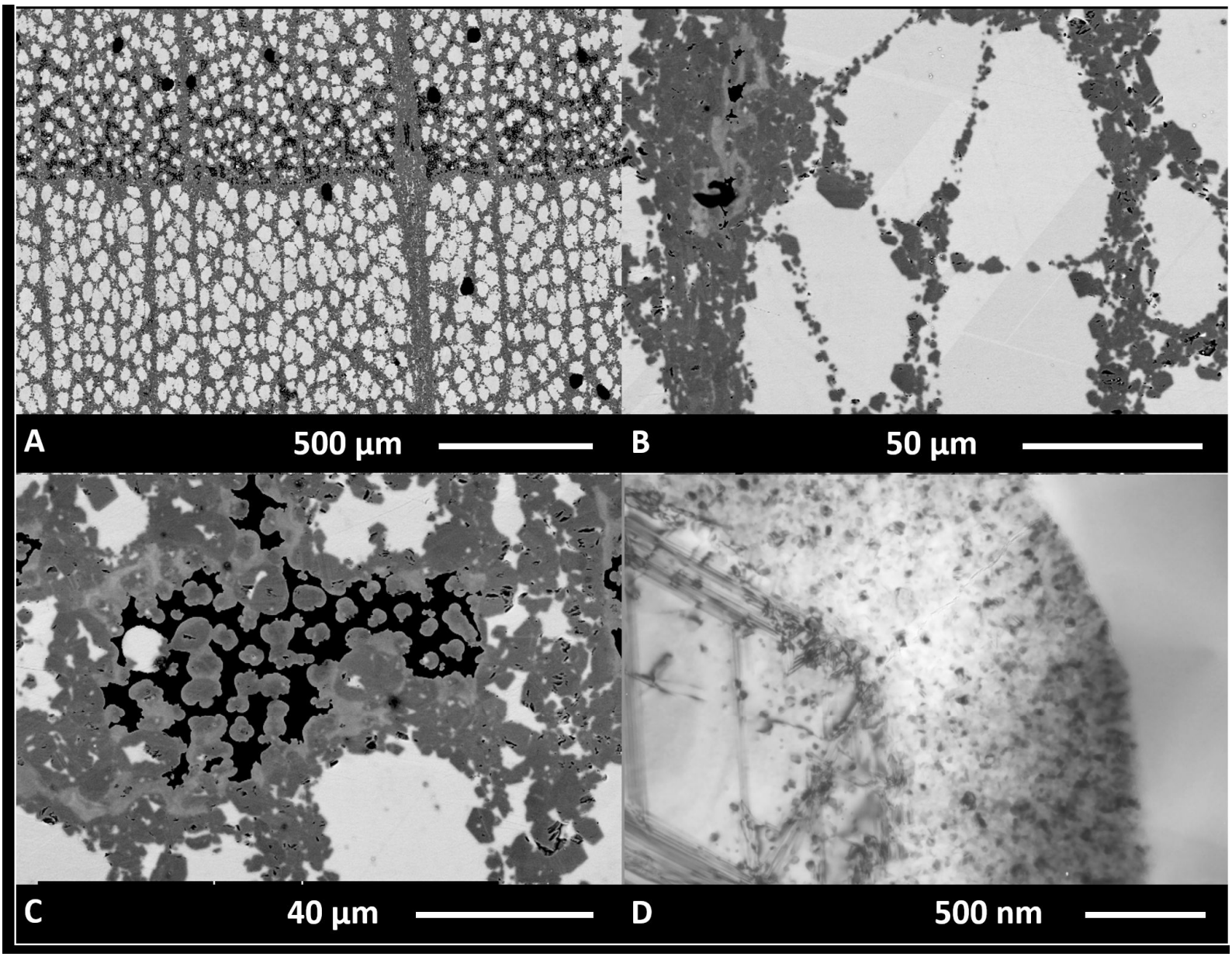

FIGURE 9

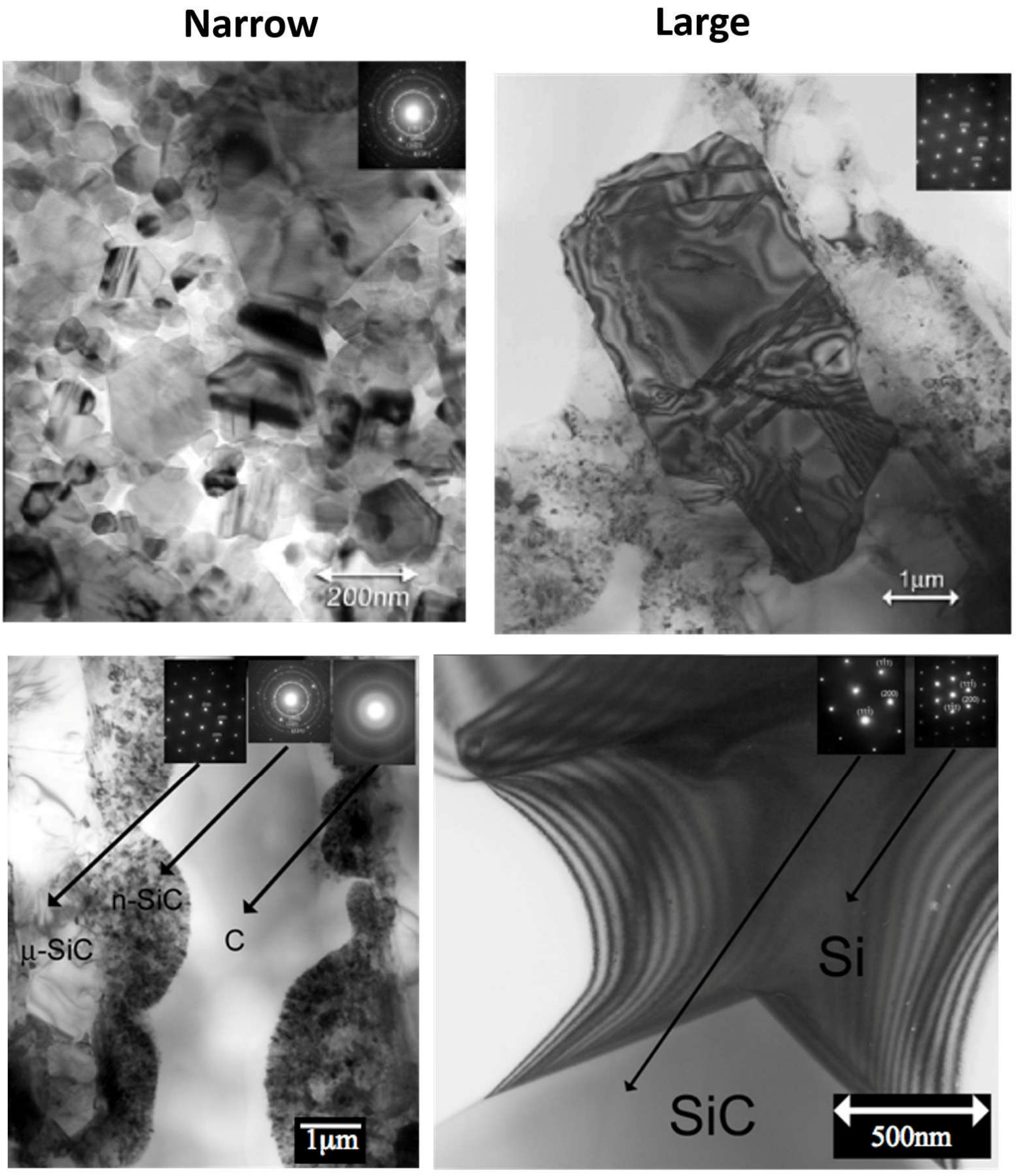

FIGURE 10

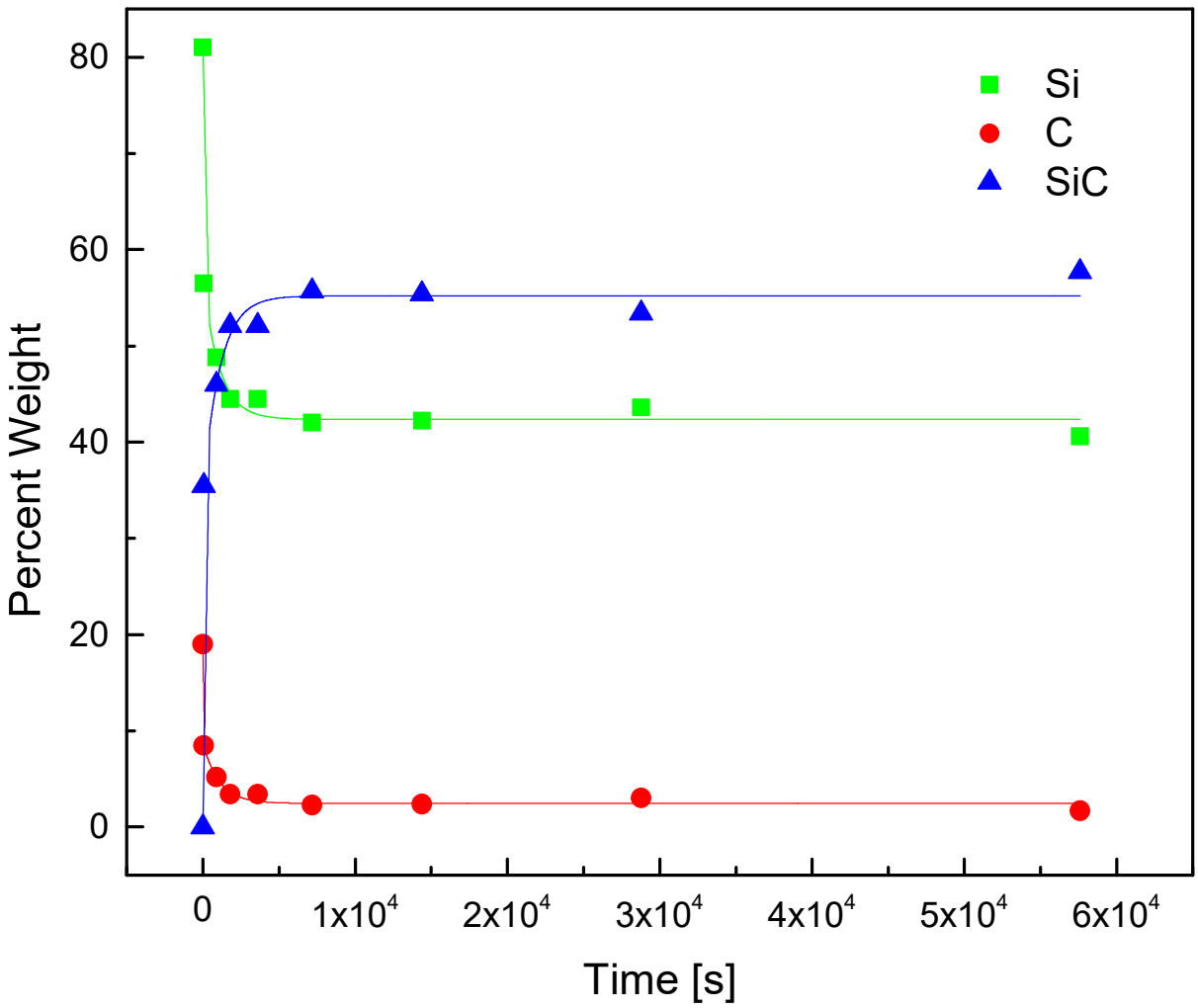
Percent Weight
Time [s]
Si
C
SiC
0
20
40
60
80
0
1x10^4
2x10^4
3x10^4
4x10^4
5x10^4
6x10^4

FIGURE 11

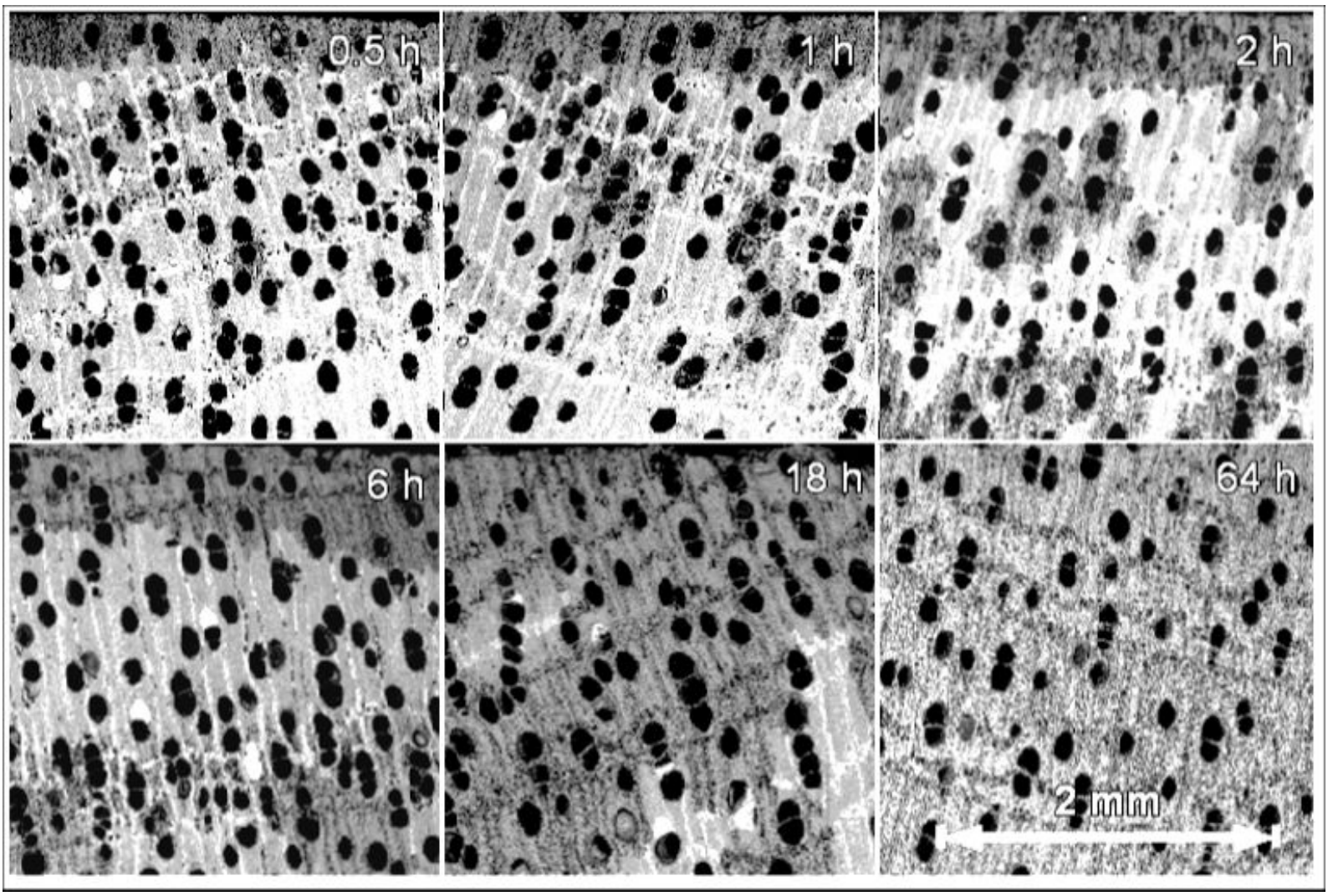

FIGURE 12

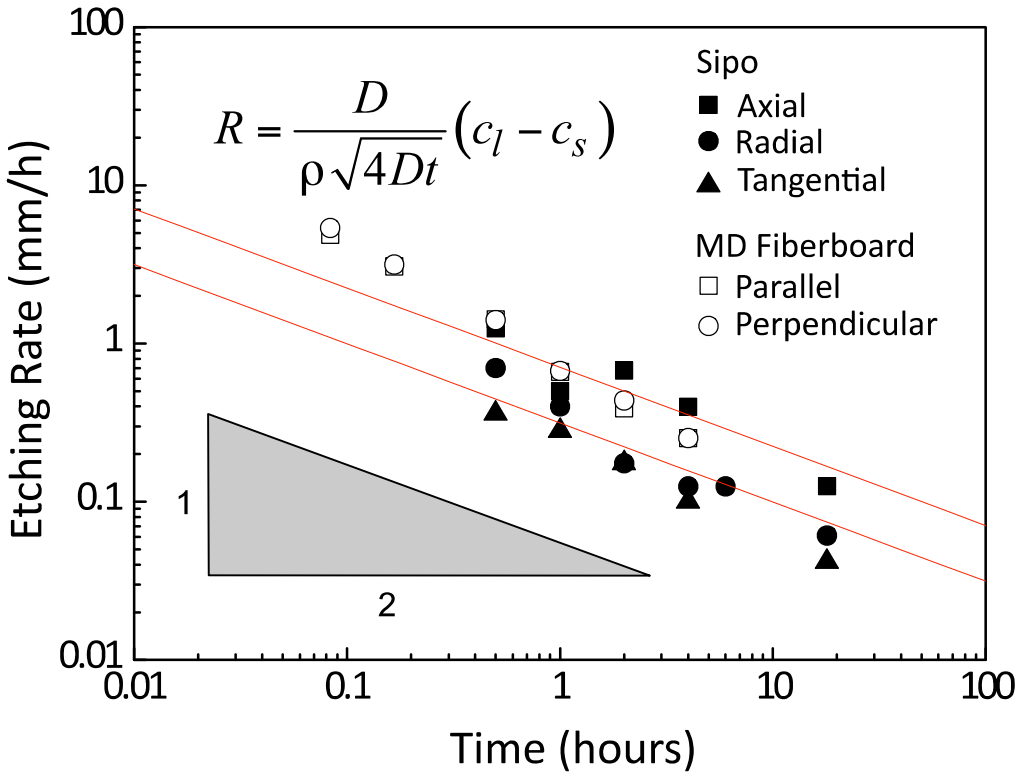
$R = \frac{D}{\rho\sqrt{4Dt}}(c_l - c_s)$
Sipo
Axial
Radial
Tangential
MD Fiberboard
Parallel
Perpendicular
1
2
Etching Rate (mm/h)
Time (hours)
100
10
1
0.1
0.01
0.01
0.1
1
10
100

FIGURE 13

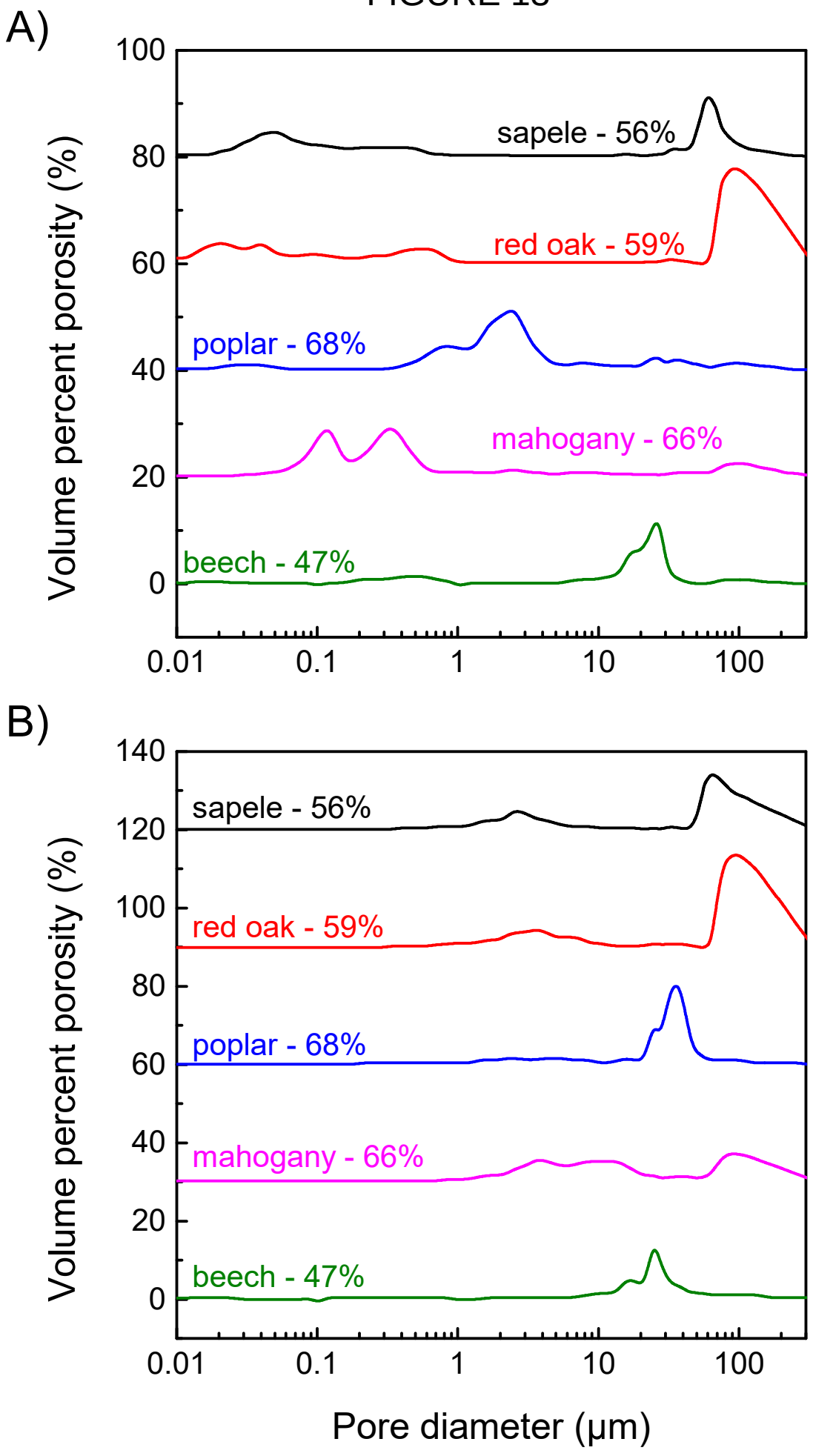
A)
100
80
60
40
20
0
Volume percent porosity (%)
sapele - 56%
red oak - 59%
poplar - 68%
mahogany - 66%
beech - 47%
0.01
0.1
1
10
100
B)
140
120
100
80
60
40
20
0
Volume percent porosity (%)
sapele - 56%
red oak - 59%
poplar - 68%
mahogany - 66%
beech - 47%
0.01
0.1
1
10
100
Pore diameter (μm)

FIGURE 14

FIGURE 15

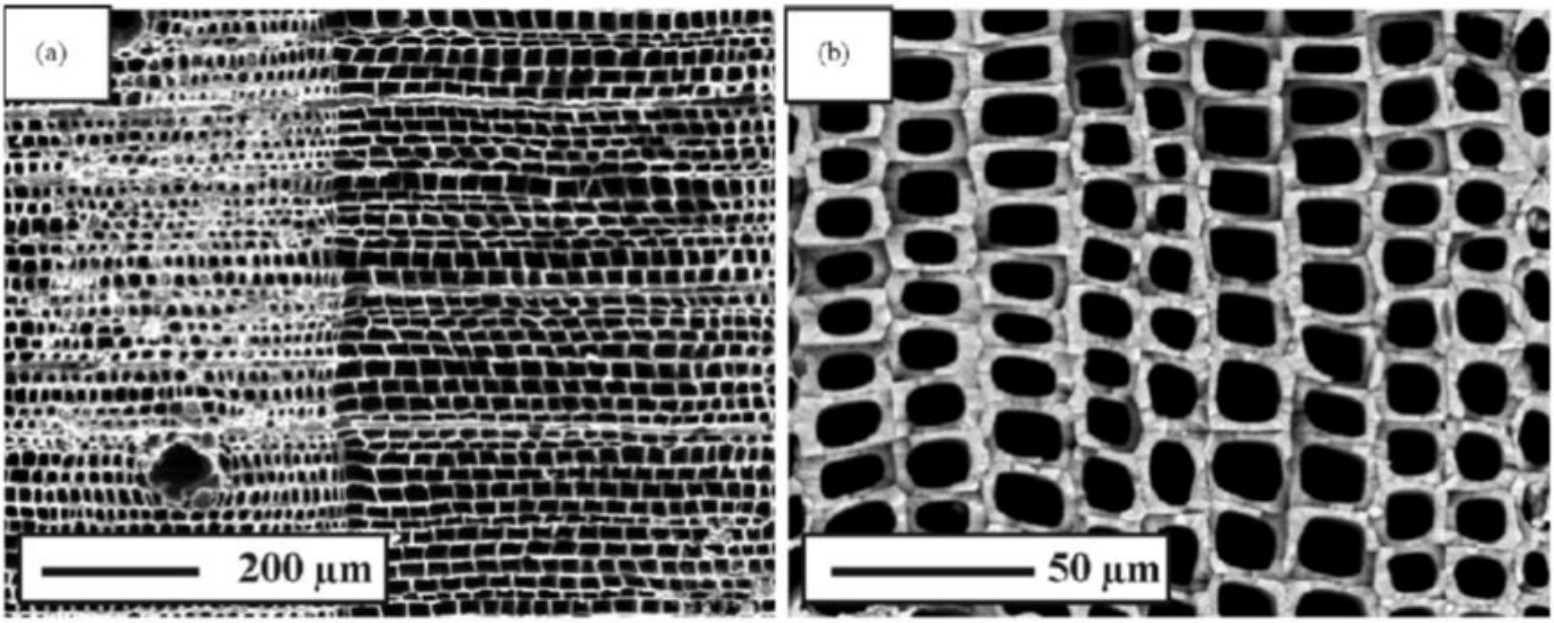

FIGURE 16

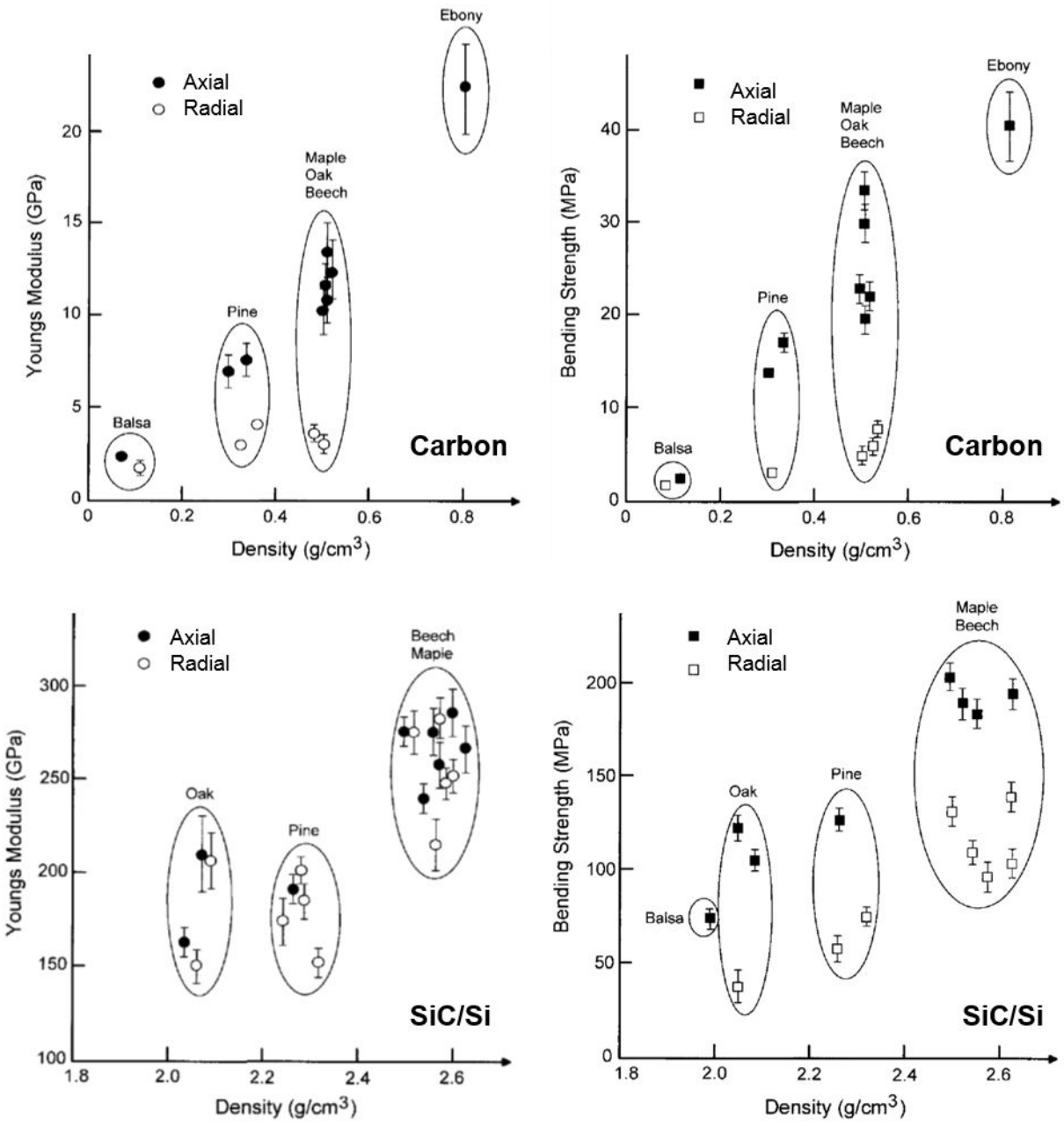
Axial
Radial
Ebony
Maple
Oak
Beech
Pine
Balsa
Carbon
Youngs Modulus (GPa)
Density (g/cm3)
Bending Strength (MPa)
Beech
Maple
Oak
SiC/Si

FIGURE 17

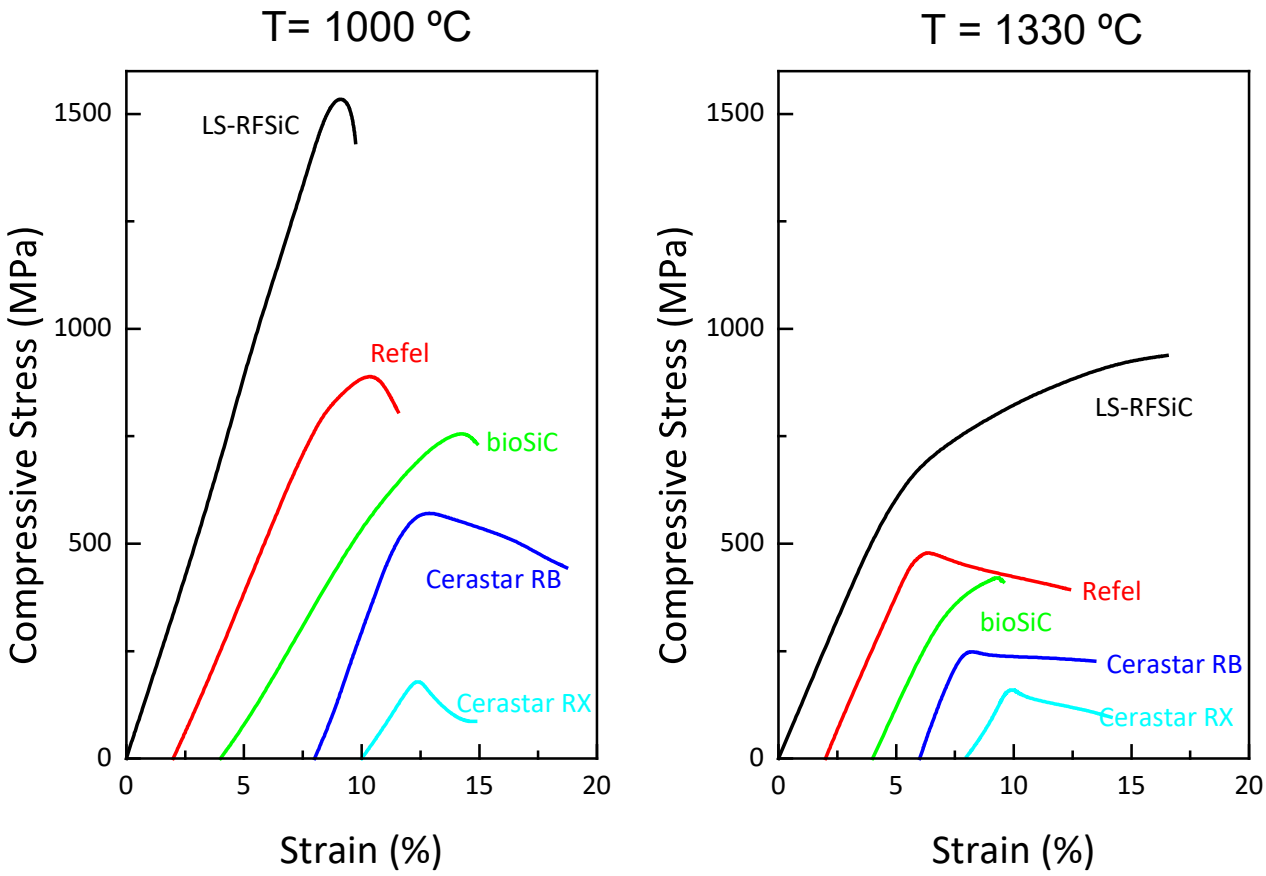
T= 1000 ºC
T = 1330 ºC
Compressive Stress (MPa)
Strain (%)
LS-RFSiC
Refel
bioSiC
Cerastar RB
Cerastar RX
0
500
1000
1500
0
5
10
15
20

FIGURE 18

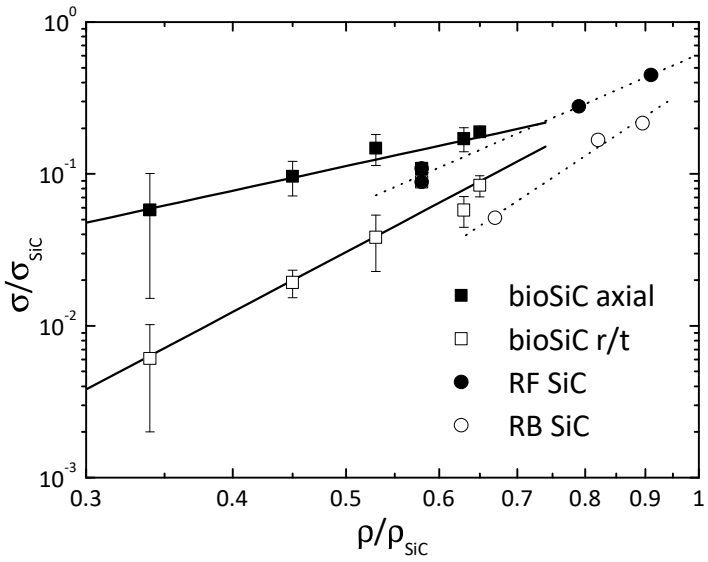
10^0
10^{-1}
10^{-2}
10^{-3}
σ/σ_{SiC}
0.3
0.4
0.5
0.6
0.7
0.8
0.9
1
ρ/ρ_{SiC}
bioSiC axial
bioSiC r/t
RF SiC
RB SiC

FIGURE 19

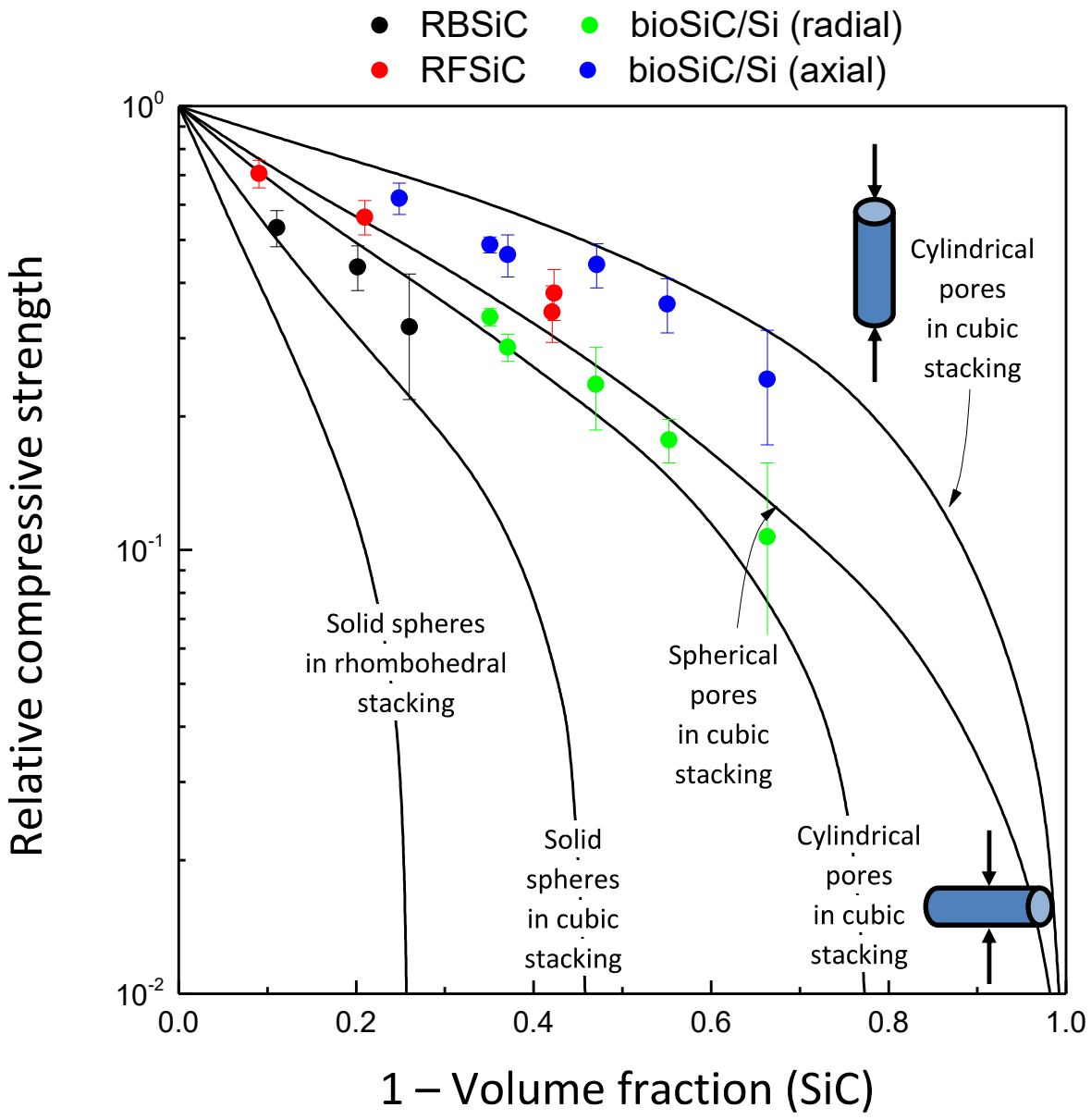
RBSiC
RFSiC
bioSiC/Si (radial)
bioSiC/Si (axial)
Relative compressive strength
1 – Volume fraction (SiC)
Cylindrical pores in cubic stacking
Solid spheres in rhombohedral stacking
Spherical pores in cubic stacking
Solid spheres in cubic stacking
Cylindrical pores in cubic stacking

FIGURE 20

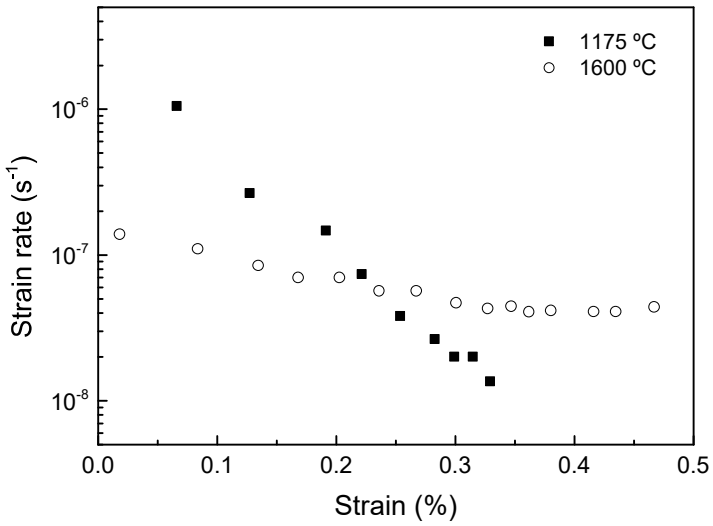
1175 ºC
1600 ºC
Strain rate (s-1)
10-6
10-7
10-8
0.0
0.1
0.2
0.3
0.4
0.5
Strain (%)

FIGURE 21